Old Dominion University
ODU Digital Commons

CCPO Publications | Center for Coastal Physical Oceanography

2008

A Modelling Study of Developmental Stage and Environmental Variability Effects on Copepod Foraging

Jerry D. Wiggert
Old Dominion University

Eileen E. Hofmann
Old Dominion University, ehofmann@odu.edu

Gustav-Adolf Paffenhöfer

Follow this and additional works at: https://digitalcommons.odu.edu/ccpo_pubs

 Part of the Marine Biology Commons, and the Oceanography Commons

Original Publication Citation

Wiggert, J. D., Hofmann, E. E., & Paffenhofer, G. A. (2008). A modelling study of developmental stage and environmental variability effects on copepod foraging. *ICES: Journal of Marine Science, 65*(3), 379-398. doi:10.1093/icesjms/fsm193

This Article is brought to you for free and open access by the Center for Coastal Physical Oceanography at ODU Digital Commons. It has been accepted for inclusion in CCPO Publications by an authorized administrator of ODU Digital Commons. For more information, please contact digitalcommons@odu.edu.

A modelling study of developmental stage and environmental variability effects on copepod foraging

Jerry D. Wiggert, Eileen E. Hofmann, and Gustav-Adolf Paffenhöfer

Wiggert, J. D., Hofmann, E. E., and Paffenhöfer, G-A. 2008. A modelling study of developmental stage and environmental variability effects on copepod foraging. – ICES Journal of Marine Science, 65: 379–398.

We used a stochastic Lagrangian model to study how behaviour contributes to copepod grazing success. The model simulates distinct foraging behaviours of *Clausocalanus furcatus*, *Paracalanus aculeatus*, and *Oithona plumifera*. Three sets of simulations were performed to investigate the effects of (a) prey-size preference; (b) variation in prey-size spectra; and (c) turbulence intensity on these species' grazing rates. The size preference simulations demonstrate that, compared with copepodites, mature females have cell ingestion rates that are an order of magnitude lower, while carbon uptake is reduced by 35%. A prey spectrum that is skewed towards cells <6 μm promotes copepodite success because the basal metabolic needs of the adult females require a prey concentration of 850–1000 cells ml^{-1}. Variations in turbulence intensity reveal distinct ecological niches, with stronger mixing favouring *O. plumifera* and stable conditions favouring *C. furcatus*. Differences in theoretically derived and simulated prey-encounter rates demonstrate that the hopping behaviour of *O. plumifera* provides an order of magnitude increase in prey encounter, whereas the feeding behaviour of *C. furcatus* can result in localized depletion of prey. These simulations highlight the importance of species-specific feeding behaviour in defining oceanic copepod distributions.

Keywords: copepod foraging, ecological niche, emergent behaviour, Lagrangian model, turbulence.

Received 14 July 2007; accepted 7 November 2007; advance access publication 25 February 2008.

J. D. Wiggert and E. E. Hofmann: Center for Coastal Physical Oceanography, Old Dominion University, 4111 Monarch Way, Norfolk, VA 23508, USA. G-A. Paffenhöfer: Skidaway Institute of Oceanography, 10 Ocean Science Circle, Savannah, GA 31411, USA. Correspondence to J. D. Wiggert: Department of Marine Sciences, University of Southern Mississippi, 1020 Balch Boulevard, Stennis Space Center, MS 39529, USA. tel: +1 228 6883491; fax: +1 228 6881121; e-mail: jerry.wiggert@usm.edu.

Introduction

Copepod grazing depends on the linked biomechanical processes of sampling method, prey perception, and size preference (Paffenhöfer, 1998). Sampling method combines foraging ambit and the means of cell acquisition (e.g. direct contact or feeding current; Price *et al.*, 1983; Bundy *et al.*, 1993), while prey perception depends on sensory cues such as hydrodynamic signals or chemical trails (Demott and Watson, 1991; Kiørboe and Thygesen, 2001). Size preference depends on developmental stage, morphological characteristics, or overall prey concentration (Nival and Nival, 1976; Landry and Fagerness, 1988; Paffenhöfer and Lewis, 1990; Hansen *et al.*, 1994). Adult copepod densities in the open ocean range from 50 to 500 ind. m^{-3} (Head *et al.*, 2002; Peralba and Mazzocchi, 2004), and each species uses some combination of prey acquisition strategies to meet its nutritional requirement.

One environmental effect known to modulate predator–prey encounter rates is small-scale fluid turbulence (Peters and Marrasé, 2000; Yamazaki *et al.*, 2002). The various copepod sampling methods are affected to different degrees by alterations in the turbulence field, which is believed to result in species distributions that track spatial variations in dissipation rate (Kiørboe and Saiz, 1995; Incze *et al.*, 2001; Visser *et al.*, 2001). A less direct effect stems from the spatial variability observed in prey-size spectra. As prey speciation shifts in response to changing environmental conditions, distinction in prey-size preference will differentially modify foraging success and growth rates of co-occurring copepod species.

Predator–prey encounter rates and planktivorous grazing are affected by variation in turbulence intensity (Rothschild and Osborn, 1988; Hill *et al.*, 1992). The typical range of the Kolmogorov length scale in marine environments is 0.3–10.0 mm (Marrasé *et al.*, 1990). The perceptive range of copepods varies notably among species and their developmental stages. As a quantifying example, this range has been estimated to be 0.5–1.4 mm for the calanoid copepod *Diaptomus sicilis* (Bundy *et al.*, 1998). Combined, these characteristic length scales suggest that planktonic organisms (5–100 μm for typical prey; 0.5–3.0 mm prosome length for typical copepods) are unlikely to experience eddy-like motions associated with oceanic turbulence directly. Instead, the prevailing understanding is that turbulence effects operate through the accompanying laminar shear (Kiørboe and Saiz, 1995; Gargett, 1997; Peters and Marrasé, 2000). Analytical models of predator–prey interaction have revealed that the response curve for variation of grazing success with turbulence intensity is dome-shaped (Mackenzie *et al.*, 1994). As turbulence intensity increases from negligible levels, the increased encounter rates lead to higher ingestion rates. However, as turbulence intensity increases further, predator response time begins to limit capture success, and a negative impact on ingestion rate manifests (Mackenzie *et al.*, 1994; Jenkinson, 1995). Other factors of prey acquisition affected by increasing intensity of small-scale

© 2008 International Council for the Exploration of the Sea. Published by Oxford Journals. All rights reserved.
For Permissions, please email: journals.permissions@oxfordjournals.org

Downloaded from https://academic.oup.com/icesjms/article-abstract/65/3/379/784056
by Old Dominion University user
on 15 May 2018

turbulence are reduced prey perception through signal degradation, feeding current alteration or disruption, and behaviour modification of both predator and prey (Marrasé *et al.*, 1990; Yen, 2000; Franks, 2001; Visser and Stips, 2002; Saiz *et al.*, 2003). Thus, the level of turbulence can differentially affect foraging success and ingestion rates of copepod species.

A Lagrangian individual-based model (IBM) that specifically includes observed foraging ambits and area(s) of perception for three copepod species has been developed (Wiggert *et al.*, 2005). The species chosen, *Clausocalanus furcatus*, *Paracalanus aculeatus*, and *Oithona plumifera*, represent three of the most common genera found in tropical/subtropical waters (Gaudy *et al.*, 2003; Huskin *et al.*, 2004; Smith and Madhupratap, 2005). *Clausocalanus furcatus* is a fast, continuous swimmer that loops repetitively, then displaces vertically before re-establishing its characteristic looping motion (Mazzocchi and Paffenhöfer, 1999). *Paracalanus aculeatus* is a slow, continuous swimmer that generates a feeding current to entrain potential food particles and perceives food at a distance by chemoreception (Paffenhöfer, 1984, 1998). *Oithona plumifera* is an ambush predator that uses its long, feathered setae to sense the hydrodynamic signals of motile particles at a distance after jumping obliquely upwards every few seconds (Svensen and Kiørboe, 2000; Paffenhöfer and Mazzocchi, 2002). Through explicit inclusion of the acquisition methods of these species, the Lagrangian IBM provided insight into how these strategies contribute to the coexistence of these three species in a dilute prey environment. The strength of this modelling approach is that it allows for emergent behaviour through the application of a fundamental rule set that is based on observed biomechanical components.

In this study, the Lagrangian IBM is used to investigate the degree to which these distinct foraging strategies allow for shifts in competitive advantage between copepod species as their environmental conditions are modified. Simulations were performed to investigate how the three species respond to variation in (i) prey-size preference that reflects differences in species morphology or developmental stage; (ii) size spectrum of the available prey field, based on observed spectra from four euphotic zone depths; and (iii) magnitude of a randomizing velocity component that encompasses the typical range of upper ocean turbulence intensities.

The emergent behaviour from these simulations provides insight into the physical and biological factors that allow for persistence and coexistence of these three copepod species. The next section provides a description of the Lagrangian model and details of the simulations performed for this study. This is followed by a description of the results. The discussion section interprets these results within the context of current understanding of how copepods function within the oligotrophic environment. The final section provides conclusions stemming from this analysis as well as some perspective regarding observational needs that would allow further development of the Lagrangian IBM.

Methods

The Lagrangian IBM simulates the time evolution of the trajectory of a given particle at location $\overrightarrow{X_i}$ by

$$\frac{\mathrm{d}\overrightarrow{X_i}}{\mathrm{d}t} = \overrightarrow{U_i}, \tag{1}$$

where the subscript denotes an individual particle (prey or copepod). The components of velocity ($\overrightarrow{U_i}$) include passive sinking speed, isotropic turbulence, and active swimming, where applicable. The foraging behaviour of the three copepods is introduced through parameterizations that include sampling ambit, area of perception (AOP), and prey perception (size preference and prey–predator separation distance). The AOP and sampling ambit are species-specific and are based on observational characterizations. For the chosen copepod species, there are two basic ambits, continuous swimming or episodic jumps with suitable directional modification applied at each time-step that results in spiralling or essentially linear motion or hops that range from vertical to horizontal. A basic state for the ambit of each species is defined; then random perturbations are applied to an individual's direction and speed at each time-step, resulting in a unique ambit for each individual within each experiment (example ambits are shown in Figure 3 of Wiggert *et al.*, 2005). A similar random perturbation of the turbulent fluid environment that affects all tracked particles is applied. Through these randomizations of the copepods' ambits and their environment, stochasticity is introduced into the simulations. Full details of the model's configuration and parameterizations, and the randomization scheme just described are given in Wiggert *et al.* (2005). The modifications to prey perception, size spectrum, and turbulence formulation newly incorporated to perform this study are detailed in the following sections.

Prey perception and size spectra

The model domain consists of a 1-l volume of water in the upper water column of the oligotrophic ocean. The initial concentration of prey (3×10^5–3×10^6 individual cells per litre) is randomly distributed throughout this domain, and each is assigned a species-based palatability ranking. For each prey item within the AOP of a given copepod, two non-dimensional prey perception factors are applied that may reduce its palatability ranking. The first perception factor (π_1) defines the range of cell sizes that are accessible to a given copepod. The observation-based cell capture efficiency developed by Bartram (1980) provides the basis for relating prey-size preference and prey diameter (d_C) as:

$$\pi_1 = \frac{(1 + \tanh[(d_c - a_1 d_P)/b_1]) \cdot (1 - \tanh[(d_c - a_2 d_P)/b_2])}{(1 + \tanh[d_P(1 - a_1)/b_1]) \cdot (1 - \tanh[d_P(1 - a_2)/b_2])}, \tag{2}$$

where the constants are $a_1 = 0.175$, $b_1 = 5.0$, $a_2 = 2.0$, and $b_2 = 4.0$. The prey-size preference parameter (d_P) in Equation (2) is varied to define the prey sizes that will not be considered for consumption.

As d_P is increased, the preferred range of cell sizes expands to include larger prey, and access to smaller cells is impaired (Figure 1), which is similar to the size-selection curves defined by Steele and Frost (1977). In this study, four values for d_P were applied (10–40 μm, in 10 μm intervals) so that the impact on carbon uptake afforded by shifts in the range of available prey sizes (Figure 1) could be assessed (see group 1 simulations described below). These curves reveal that, at higher values of d_P, access to larger cells is significantly extended, whereas access to cells with d_C less than 10 μm is curtailed or eliminated. These shifts in preferred prey size represent different stages of copepod growth, with the maximum value of d_P coinciding with mature females.

Downloaded from https://academic.oup.com/icesjms/article-abstract/65/3/379/784056
by Old Dominion University user
on 15 May 2018

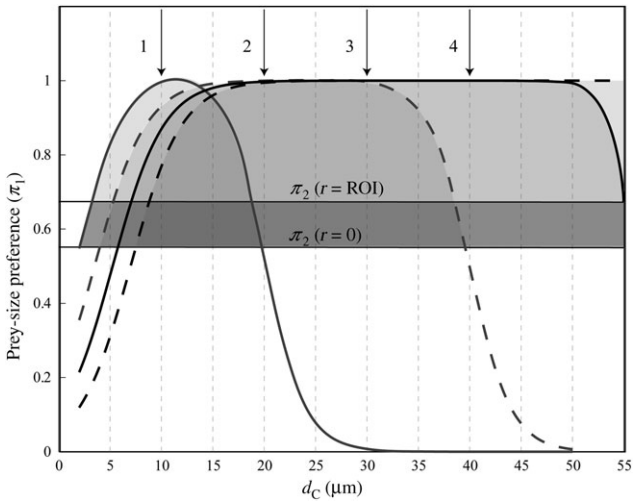

Figure 1. Size preference curves as a function of prey perception (π_1) and cell diameter (d_C). The four size preference curves use values of the prey-size preference parameter (d_P) in Equation (2) of (1) d_P = 10 μm (grey solid line); (2) d_P = 20 μm (grey dashed line); (3) d_P = 30 μm (black solid line); and (4) d_P = 40 μm (black dashed line). The curves prescribe how the size range of grazed cells evolves with copepod developmental stage, with the largest value of d_P corresponding to adult females and the smallest value corresponding to the youngest copepodites. The maximum range in prey size for each stage occurs where the size preference curve intersects the lower horizontal line, which is where there is no separation between the copepod and its prey [$\pi_2(r = 0)$]. These ranges are (1) 2.0–19.8 μm (d_P = 10 μm), (2) 4.0–39.6 μm (d_P = 20 μm), (3) 5.8–59.6 μm (d_P = 30 μm), and (4) 7.6–79.6 μm (d_P = 40 μm). The upper horizontal line corresponds to the maximum perception distance between the copepod and its prey [$\pi_2(r$ = ROI)] and illustrates how the accessible size range is reduced when prey are at the AOP boundary. The shading under the preference curves emphasizes where the accessible cell sizes for the four developmental stages are distinct and where they overlap.

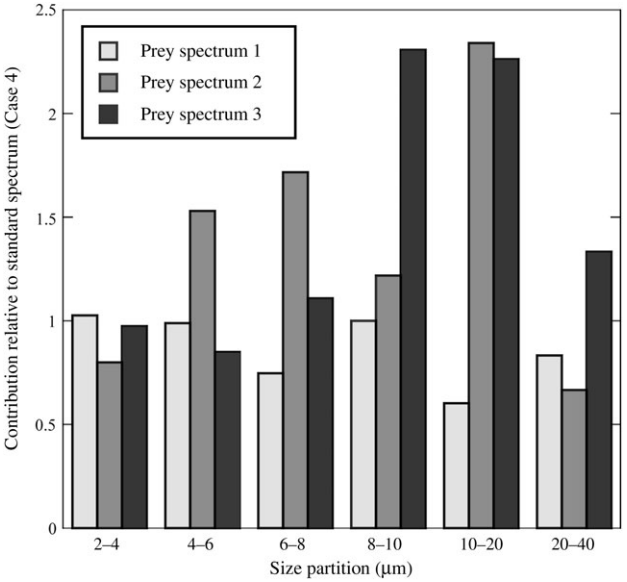

Figure 2. The three alternative prey spectra used in simulation group 2. These spectra have been normalized by spectrum 4, which is taken as the standard condition because it is the individual spectrum that corresponds most closely to the mean of all prey spectra obtained from observations of Paffenhöfer *et al.* (2003). Spectrum 1 is from within the surface mixed layer (15 m) and is shifted towards cells with ESD $<$10 μm. Prey in the 4–6 μm and 6–8 μm size partitions are most pronounced in spectrum 2, which is within the seasonal thermocline (105 m) and above the DCM. Spectrum 3 is also from the seasonal thermocline (75 m) and features elevated prey concentrations in the 8–10 μm and 20–40 μm size partitions.

The second perception factor (π_2) linearly reduces prey palatability with distance from the copepod. This is applied as $\pi_2 = 1.0-0.2(r/\mathrm{ROI})$, where r is prey–predator distance and ROI is the radius of influence (see Figure 1 and Table II in Wiggert *et al.*, 2005). Thus, π_2 ranges down to 0.8 at the AOP boundary, whereas π_1 ranges from 0 to 1 (Figure 1). The initial palatability ranking for each potential prey within a copepod's AOP is multiplied by both π_1 and π_2. If its resulting rank remains above a prescribed threshold, the particle is consumed (details of this ranking procedure are given in Wiggert *et al.*, 2005). In Figure 1, the two horizontal lines [$\pi_2(r = 0)$ and $\pi_2(r = \mathrm{ROI})$] illustrate how the range of accessible prey sizes is effectively reduced when prey are at the limits of a copepod's AOP.

In this study, four prey spectra from the Sargasso Sea (Paffenhöfer *et al.*, 2003) are used to investigate how variation in prey-size distribution affects carbon uptake and grazing success of the model's copepod species (see group 2 simulations, described below). Spectrum 1 is from 15 m and within the surface mixed layer (Figure 2, Table 1). The sample depths for the other three spectra range from 75 to 140 m and are all within the seasonal pycnocline. For these three profiles, the depth of the deep chlorophyll maximum (DCM) is ~120 m. Thus, the prey fields represented in spectra 2 and 3 are above the DCM, whereas the one associated with spectrum 4 lies below it (see Figure 2 in Paffenhöfer *et al.*, 2003). Spectrum 4 is taken as the standard prey field, because it most closely adheres to the mean distribution for all measured spectra. Prey spectrum 1 has fewer cells with equivalent spherical diameter (ESD) $>$10 μm and, in particular, the lowest contribution by the 10–20 μm partition. Spectrum 2 is distinguished by the predominance of cells in the 4–8 μm range, and cells $>$8 μm ESD are most prominent in spectrum 3 (Figure 2). For the latter two spectra, the 10–20 μm partition is

Table 1. Percentage contribution (C^*) to total prey population by partition for the four prey spectra.

Prey partition (mm)	Spectrum 1	Spectrum 2	Spectrum 3	Spectrum 4
2–4	0.7650	0.5957	0.7264	0.7452
4–6	0.1732	0.2679	0.1488	0.1751
6–8	0.0359	0.0824	0.0532	0.0480
8–10	0.0169	0.0206	0.0390	0.0169
10–20	0.0085	0.0330	0.0319	0.0141
20–40	0.0005	0.0004	0.0008	0.0006

Spectrum 1 (Cast 11a, 15 m), spectrum 2 (Cast 35, 105 m), spectrum 3 (Cast 41, 75 m), and spectrum 4 (Cast 11a, 140 m) were determined from *in situ* water samples obtained during early summer 2001 in the southwest Sargasso Sea (Paffenhöfer *et al.*, 2003). The total concentration (C_T) used in these simulations was 300, 533, 950, 1700, and 3000 cells ml^{-1}. The number of prey within the six prey partitions is determined by multiplying C^* by the C_T needed for a given simulation.

Downloaded from https://academic.oup.com/icesjms/article-abstract/65/3/379/784056
by Old Dominion University user
on 15 May 2018

more than 100% greater than in the standard spectrum. These prey spectra maximize the contrast in the 10–20 μm size class. To obtain a prey field when a given simulation is initialized, the values of the percentage of total prey population (C^* in Table 1) are multiplied by the total cell concentration (C_T).

Impact of turbulence

Simulated prey motion consists of sinking and stochastic fluid motions (i.e. small-scale turbulence) with velocity magnitudes that are typical of isotropic turbulence within the surface mixed layer or pycnocline. Fluid motions on larger spatial scales (e.g. geostrophic flows or internal wave oscillations) are not included because they impact all particles equally. Particle sinking (w_s) is determined for each individual cell using a modified form of the Stokes equation, which includes a randomizing modification to cell density that is representative of natural variability within the plankton population [see Equation (2) in Wiggert *et al.*, 2005]. The turbulence velocity ($\vec{u}_D$) contributes a random component to the velocity vector of each copepod and planktonic prey. It is applied as a maximum speed (U_D), the magnitude of which is modified for each direction by a set of random amplitude coefficients ($\vec{\beta}^R$) that are uniformly distributed between −1 and 1 as:

$$\vec{u}_D = \vec{\beta}^R U_D. \tag{3}$$

A new set of $\vec{\beta}^R$ is determined for each individual at every time-step. The value of U_D is held constant throughout a simulation. For simulations that investigate turbulence effects on predator–prey encounter rate (see group 3 simulations described below), U_D was varied over 0.1–6.0 mm s^{-1}, which encompasses the range associated with wind-driven turbulence within the upper ocean (Mackenzie *et al.*, 1994; Jiménez, 1997; Maar *et al.*, 2003). Because values of $\vec{\beta}^R$ are randomly determined, the energy spectrum of $\vec{u}_D$ is white, which is clearly inconsistent with the well-known red spectrum characteristic of isotropic turbulence (e.g. Lesieur, 1987). However, this model study focuses on how copepod foraging is affected by variations in the intensity of fluid perturbation over a realistic range in magnitude. Thus, accurate representation of the distribution of turbulence velocities within the mixed layer or upper thermocline was not necessary.

An analytical method for quantifying the effect of small-scale turbulence on predator–prey encounter was introduced by Rothschild and Osborn (1988) and subsequently refined by Evans (1989). These studies provide the following general expression for encounter rate (Z_A) between a predator (copepod with speed U_C) and prey within a given size partition (with speed U_P and concentration C_P) under the influence of turbulence of the form:

$$Z_A = \pi r_P^2 C_P \left(U_P^2 + U_c^2 + 2\left|\vec{u}_D\right|^2 \right)^{1/2}, \tag{4}$$

where r_P is the predator's radius of perception based on its perceived volume when stationary (cf. Table II in Wiggert *et al.*, 2005) and $\vec{u}_D$ [Equation (3)] is the turbulence r.m.s. velocity for particles separated by a distance $O(C_T^{-1/3})$. Parameter definitions and resulting values of Z_A for the three copepod species are given in Table 2.

Simulation details

In all simulations, ten copepods of the same species were introduced into the model domain, and between six and eight one-hour simulations were performed at each value of C_T (300, 534, 950, 1700, and 3000 cells ml^{-1}) for a given set of prey accessibility or environmental conditions (see simulation groups defined below). Ten individuals per simulation yields 60–80 realizations for each set of conditions and allows calculation of statistics to assess the stochastic effects of initial prey distribution, foraging ambits, and imposed turbulence velocities. As noted below, the model tracks carbon uptake through cell ingestion. However, copepod growth is not simulated, and an individual's size remains fixed over the duration of these short simulations. The model boundaries are periodic so that any particle exiting one side of the 1-l volume reappears on the opposite side, which prevents loss of prey or an accumulation at the base of the model domain.

Two foraging-related rates calculated from the simulations were used as diagnostic variables. The first, encounter rate (Z_M), was determined by summing the eaten and uneaten occurrences for the prey. When repeated, uneaten encounters occurred for a given cell over a finite succession of time-steps (usually ≤4), only the first was counted as a distinct uneaten encounter in the

Table 2. Theoretical encounter rate (Z_A, in cells h^{-1} $ind.^{-1}$) calculated for two turbulence intensity conditions ($|\vec{u}_D| = 0$ and 6.5 mm s^{-1}) using Equation (4) and a total prey concentration (C_T) of 300 cells ml^{-1}.

Prey partition (mm)	Prey velocity ($U_P \times 10^{-3}$, mm s^{-1})	Turbulence intensity ($|\vec{u}_D|$, mm s^{-1})					
		C. furcatus		*P. aculeatus*		*O. plumifera*	
		0.0	6.5	0.0	6.5	0.0	6.5
2–4	0.072	1 552	5 417	872	5 417	92	2 814
4–6	0.200	365	495	205	1 273	22	661
6–8	0.392	100	136	56	349	6	181
8–10	0.648	35	48	20	123	2	64
10–20	1.800	29	40	17	102	2	53
20–40	7.200	1	2	1	4	0	2
Total Z_A (all prey partitions)		2 082	6 137	1 171	7 269	123	3 776

The partition-specific prey density [C_P, Equation (4)] is obtained by multiplying C_T by C^* of prey spectrum 4 (Table 1). Prey velocity (U_P) is also partition-specific and based on the sinking velocity (w_S) calculated using the partition's median cell diameter. Values of U_C are from Table I in Wiggert *et al.* (2005).

Downloaded from https://academic.oup.com/icesjms/article-abstract/65/3/379/784056
by Old Dominion University user
on 15 May 2018

determination of Z_M. The others were disregarded because they represent an artefact of the discretized nature of numerical simulations. The second diagnostic is ingestion rate (I, cells h^{-1} ind.$^{-1}$), which can also be used to calculate copepod carbon uptake (ng C h^{-1} ind.$^{-1}$) by applying the cell diameter (d_C) that is tracked for each individual prey. The transformation to carbon content is accomplished through use of the relation determined by Verity *et al.* (1992), the assumption of sphericity, and constant stoichiometry (i.e. variation in nutritional quality of prey is not included). The basal metabolic rate for each copepod species was estimated using the relations determined by Ikeda (1985) that apply a mean animal weight and a water temperature of 20°C. This rate provides a baseline for assessing the relative increase or decrease in carbon uptake in the various simulations. The ratio of ingestion rate to encounter rate (I:Z_M) gives a measure of the efficiency of ingestion.

Three groups of simulations were performed. Simulation group 1 consists of varying the size range of preferred prey by modifying d_P from 10 to 40 μm in 10 μm increments [Equation (2)]. The maximum value of d_P was the standard condition used in Wiggert *et al.* (2005) and represents adult females. The shift in preferred prey size associated with lowering d_P is a parameterization for developmental-stage-related differences in foraging behaviour. Shifting the preference curve in this manner provides for transition from young copepodites to mature adult females. For the other two simulation groups, only the smallest (10 μm) and largest (40 μm) values of d_P are applied, and results are reported as associated with copepodites and adult females, respectively. Simulation group 2 consists of applying four prey spectra with distinct size distributions (Figure 2, Table 2). Imposing the four prey distributions allows us to investigate the effects of natural variation in prey-field composition on grazing rate. Simulation group 3 consists of applying individually randomized velocities [U_D in Equation (3)], within a prescribed range of relatively low magnitude, to all prey. The stochastic velocity field represents small-scale isotropic turbulence, and varying the range of turbulence velocities simulates conditions typical of the upper pycnocline and those of the surface mixed layer.

Results

Simulation group 1: prey-size preference as a proxy for copepod developmental stage

Rates of individual and mean carbon uptake are strongly affected by shifts in prey-size preference (Figure 3). The carbon uptake rate for *C. furcatus* (top row, Figure 3) increases with increasing forage. The range of simulated carbon uptake rates falls within the range of observed rates (Figure 3). Similar trends in the simulated carbon uptake rate were obtained for *P. aculeatus* (middle panels) and *O. plumifera* (bottom row). For all prey densities and copepod species, the range of the individual carbon uptake rates expands as d_P increases. Thus, as size preference shifts towards large cells, successfully obtaining nutritional needs is increasingly hit or miss because cells with ESD >8 μm make up only 2.5–7% of

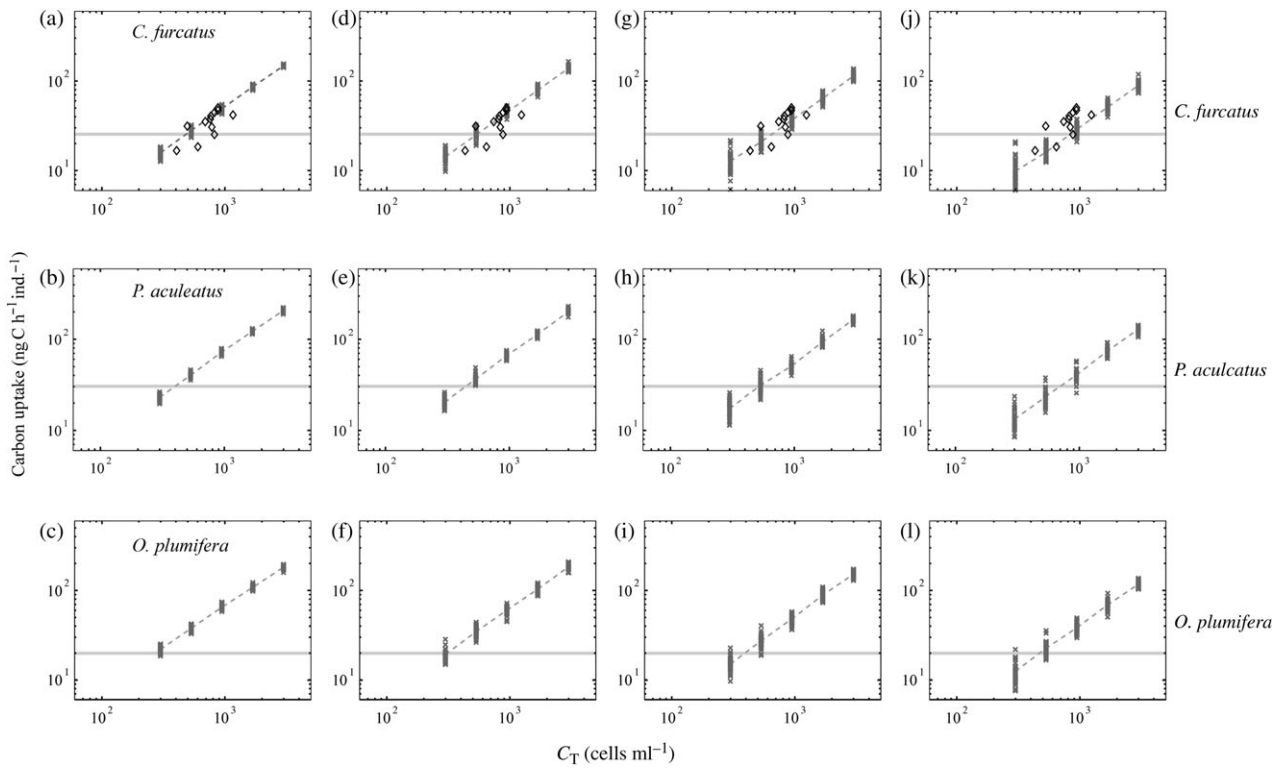

Figure 3. Carbon uptake (ng C h^{-1} ind.$^{-1}$) as a function of total cell concentration (C_T) for the four developmental stages for the size-preference curves (Figure 1) obtained with d_P equal to (a–c) 10 μm, (d–f) 20 μm, (g–i) 30 μm, and (j–l) 40 μm. The simulated mean ingestion rate (dashed line) and results for each individual simulation (cross) are shown. Based on observed weights (Table 1 in Wiggert *et al.*, 2005) and a temperature of 20°C, each copepod's basal metabolic rate (horizontal line) was estimated using the method of Ikeda (1985). These values are (a) 25.4, (b) 30.2, and (c) 19.6 ng C h^{-1} ind.$^{-1}$. Measured carbon uptake rates for *C. furcatus* (diamond) reported in Paffenhöfer *et al.* (2006) are shown for comparison.

Downloaded from https://academic.oup.com/icesjms/article-abstract/65/3/379/784056
by Old Dominion University user
on 15 May 2018

the prey population (Table 1). This trend is accentuated at low C_T (total prey concentration, cells ml^{-1}). The other trend apparent in these results is that, as d_P increases, mean carbon uptake steadily decreases for all C_T (Figure 3). Between $d_P = 10$ and 40 μm at maximum C_T, the decrease in mean carbon uptake is 58 ng C h^{-1} ind.$^{-1}$ for *C. furcatus*, 78 ng C h^{-1} ind.$^{-1}$ for *P. aculeatus*, and 64 ng C h^{-1} ind.$^{-1}$ for *O. plumifera*. It is interesting that the magnitude of carbon uptake at $d_P = 10$ μm for these species (147 ± 3, 207 ± 9, and 181 ± 7 ng C h^{-1} ind.$^{-1}$, respectively) is not statistically different from instances when $d_P = 20$ μm. However, for all three species, the error bars are doubled.

Considerable differences are apparent in each species' success at achieving basal levels of carbon uptake at low C_T and $d_P = 10$ μm. *Clausocalanus furcatus* requires a prey density greater than 480 cells ml^{-1} to obtain its basic metabolic needs, whereas *P. aculeatus* meets these at ~400 cells ml^{-1}, and *O. plumifera* can attain its basic requirements at 300 cells ml^{-1} (Figure 3a–c). Extrapolating from the intercept of the mean uptake curve with the minimal metabolic condition, the prey concentration necessary for all three species to meet their basal needs increases by 65–75% between $d_P = 10$ and 40 μm (Figure 3). For *C. furcatus*, the lowest prey concentration yields a number of individual carbon uptake rates at larger values of d_P that exceed all of those obtained when $d_P = 10$ μm (Figure 3a, d, g, and j). However, with increasing d_P, it is clear that the mean rate of carbon uptake decreases monotonically. In contrast, for *P. aculeatus* (Figure 3b and k) and *O. plumifera* (Figure 3c and l), the maximal individual rate demonstrates a consistent decrease between the smallest and largest values of d_P.

The carbon uptake rate is determined by carbon content of grazed cells and the rate at which these cells are ingested. The latter is bounded by the preyen counter rate, which may be reduced by multiple encounters with the same cell. The cell-encounter rate and ingestion are linked through copepod perception, degree of satiation, cell size and predator–prey distance (Figure 1), and biomechanical limits, such as prey processing time. As expected, the simulated encounter rate for each species depends on C_T and is essentially independent of d_P (Figure 4a–c). At a given cell concentration, the encounter rate varies within a factor of 2 for the three copepod species (Figure 4). Over the full range of size preference, the ingestion rate for each species exhibits a range of more than an order of magnitude at a given C_T (Figure 4d–f). The lower values of ingestion rate coincide with the preference shift towards large prey with higher nutritional content and limited access to small cells. In addition, the ingestion rate reveals a consistent linear dependence with cell concentration for all values of d_P, except for some curvature at the higher cell concentrations that is only apparent when $d_P = 10$ μm. This change in

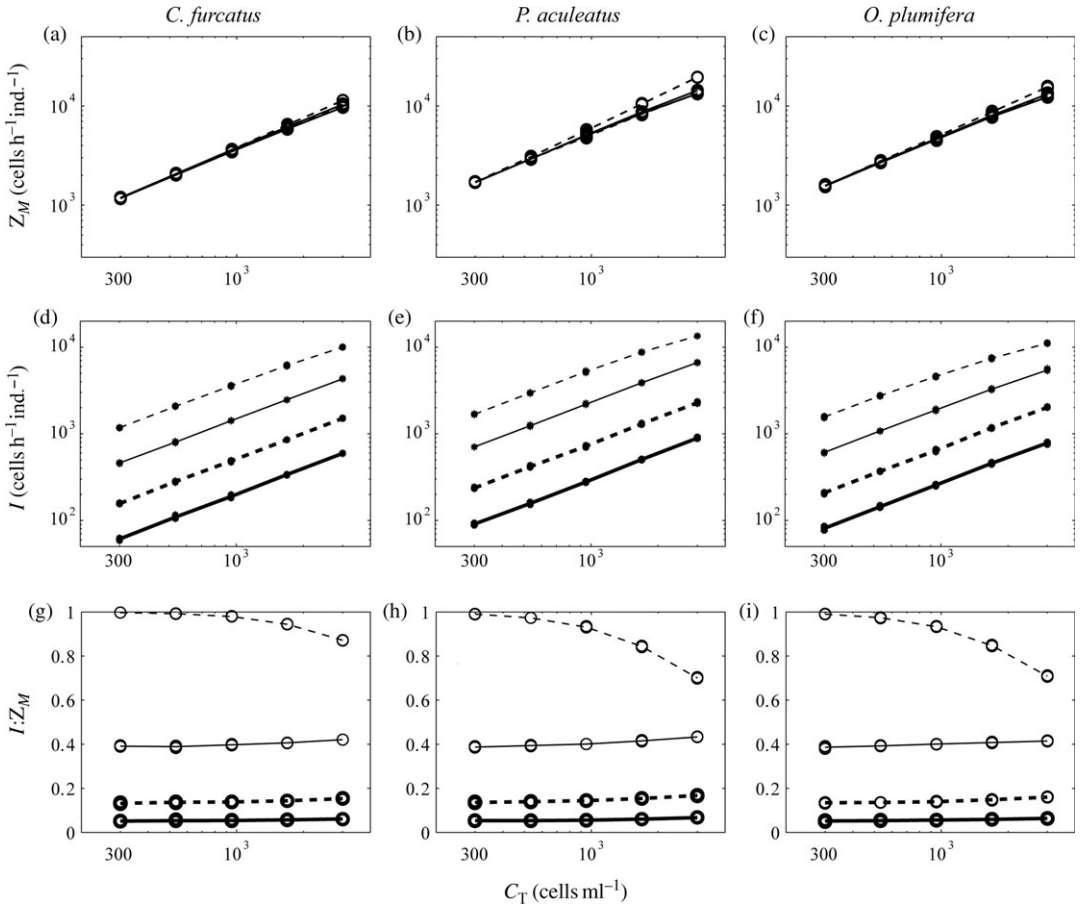

Figure 4. Simulated encounter rate (Z_M, cells h^{-1} ind.$^{-1}$; panels a–c), ingestion rate (I, cells h^{-1} ind.$^{-1}$; panels d–f), and I:Z_M (panels g–i) as a function of total cell concentration (C_T) for *C. furcatus* (left column), *P. aculeatus* (middle column), and *O. plumifera* (right column). Results are shown for size preference parameter (d_P) values of 10 μm (dashed line), 20 μm (solid line), 30 μm (heavy dashed line), and 40 μm (heavy solid line).

Downloaded from https://academic.oup.com/icesjms/article-abstract/65/3/379/784056
by Old Dominion University user
on 15 May 2018

slope with increasing cell concentration occurs because the ingestion rate is approaching a plateau beyond which increased prey concentration has little effect.

When $d_P = 10$ μm, essentially all of the encountered cells are grazed at the lowest values of C_T, whereas at maximal C_T, 70% (*P. aculeatus*) to 85% (*C. furcatus*) of the encountered cells are consumed (Figure 4g–i). This reduction in the ratio of ingestion to encounter rate ($I{:}Z_M$) with increasing prey concentration is the result of the plateau in ingestion rate (Figure 4d–f). For the other three values of d_P, $I{:}Z_M$ is comparable for all three species of copepod and essentially constant with increasing cell concentration (Figure 4g–i). A slight increase occurs at the highest cell concentrations, with this increase being a consequence of the slightly reduced encounter rates at these concentrations (Figure 4a–c). The variation in encounter rate at high prey concentration is likely an artefact of the means of tallying encounters (described under the heading "Impact of turbulence"), because no adjustment has been made for ingested cells that were not eaten in immediately preceding time-steps. Thus, the encounter rates (Figure 4a–c) may be slightly inflated, especially at high cell concentrations when $d_P = 10$ μm. An upper bound for this artefact can be ascertained by subtracting I ($d_P = 40$ μm) from I ($d_P = 10$ μm), which gives a range of $2–9 \times 10^3$ cells h^{-1} ind.$^{-1}$ over all C_T (Figure 4d–f).

The percentage of carbon contributed by individual prey-size partitions reveals that contributions differ by only 2–3% for all size preferences and partitions for the three species (Figure 5). With $d_P = 10$ μm, the 2–4 and 4–6 μm partitions each provide 22–24% of the total diet, whereas the larger sizes are monotonically less prominent. Overall, the 10–20 μm partition provides 30% of the uptake (i.e. ~6% per 2 μm partition) and, as expected,

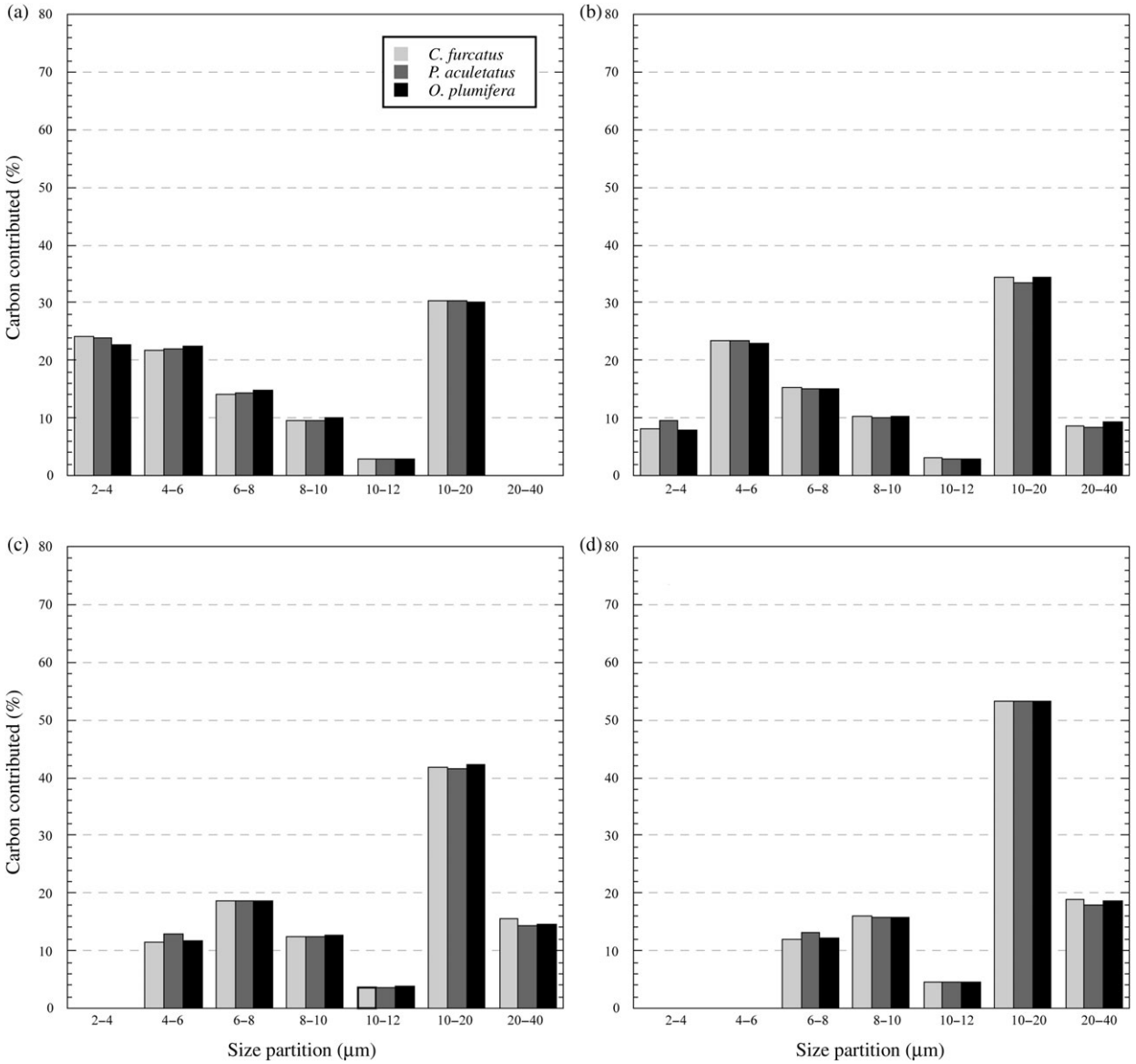

Figure 5. Percentage of total carbon uptake provided to each copepod species by prey within seven size partitions obtained for size preference parameter (d_P) values of (a) 10 μm, (b) 20 μm, (c) 30 μm, and (d) 40 μm. The partition definitions are consistent with those listed in Table 1. The 10–12 μm partition is also shown to underscore the drop-off in contribution within bins with 2 μm increments.

Downloaded from https://academic.oup.com/icesjms/article-abstract/65/3/379/784056
by Old Dominion University user
on 15 May 2018

there is no contribution from the 20–40 μm partition (Curve 1, Figure 1). With $d_P = 20$ μm, the contribution from the 2–4 μm partition drops to 8–10%, whereas the 4–6 μm partition is unchanged. Indeed, it is interesting that the four intermediate size partitions appear to allow the effect of the increase in d_P to "pass through" to the two largest partitions (Figure 5b). Thus, the primary compensation to the reduced grazing on small cells is provided by the 20–40 μm partition, which contributes ~8% to the total diet, with the 10–20 μm partition increasing slightly to ~34%.

With $d_P = 30$ μm, the 2–4 μm partition no longer contributes, the contribution of the 4–6 μm partition is reduced by half, and the 6–8 μm partition increases to 18% and becomes the dominant small-cell diet source (Figure 5c). The most pronounced increase occurs in the 10–20 μm partition, which contributes 42% of the total diet, whereas the 20–40 μm partition rises to 14%. With $d_P = 40$ μm, the 4–6 μm partition is also eliminated, whereas contributions from the 10–20 and 20–40 μm partitions increase to 53% and 18% of the total carbon uptake, respectively (Figure 5d). These percentage contribution characterizations apply over a range of cell concentrations. However, for individual values of C_T, no trend is apparent (not shown), which indicates that perception is the factor determining the relative contribution of a given size prey to the total diet.

Simulation group 2: prey-size spectra

Dependence of mature females on distribution of prey size

With $d_P = 40$ μm, the two smallest size partitions are completely eliminated, whereas the 6–8 μm partition contributes only marginally to the copepod diet (Figure 1). For this preference curve, prey spectrum 1 results in a significantly reduced likelihood that the basal metabolic rates of any of the three species will be met (Figure 6a–c). The mean carbon uptake rates indicate that attainment of metabolic needs requires 35–55% higher prey concentrations, with *O. plumifera* exhibiting the most pronounced change (Figure 3l vs. Figure 6c). Moreover, *C. furcatus* and *P. aculeatus* require prey concentrations above 10^3 cells ml^{-1} (Figure 6a and b). The combination of fewer prey in the 10–20 μm partition and the minimal contribution to the adult diet from cells <8 μm ESD results in the 8–10 μm partition making a greater contribution to the total carbon uptake than obtained for the standard prey spectrum (24% vs. 16%, Figures 5d and 7a), despite accounting for an equivalent proportion of the prey population (Figure 2). Thus, the overall reduction in carbon uptake resulting from prey spectrum 1 is a direct consequence of the reduced contribution made by large cells to the overall diet.

For the size distributions in prey spectra 2 and 3, there is little difference in carbon uptake rate for the three species, and all meet basic metabolic costs at prey concentrations of 500 cells ml^{-1} or less (Figure 6d–i). This represents a reduction of 35–40% in the

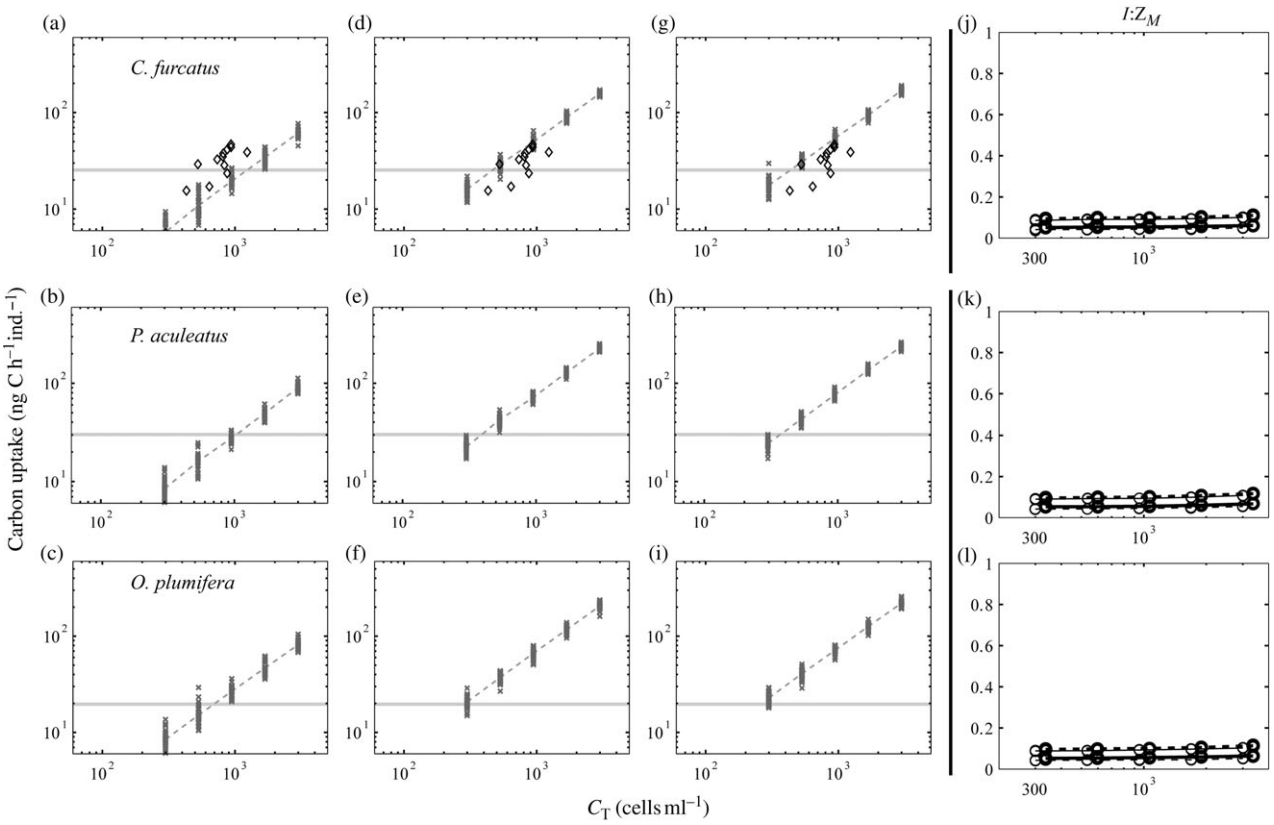

Figure 6. Simulated carbon uptake (ng C h^{-1} ind.$^{-1}$) as a function of total cell concentration (C_T) for the mature females ($d_P = 40$ μm) obtained for (a–c) prey spectrum 1, (d–f) prey spectrum 2, and (g–i) prey spectrum 3. Equivalent results obtained using the standard prey distribution (spectrum 4) are shown in Figure 3j–l. The ingestion-to-encounter-rate ratio ($I{:}Z_M$) (j–l) for prey spectrum 1 (dashed line), prey spectrum 2 (solid line), prey spectrum 3 (heavy dashed line), and prey spectrum 4 (heavy solid line) are also shown. The results for prey spectra 3 and 4 have been horizontally offset so that they are distinguishable from prey spectra 1 and 2, respectively. Other details are as described for Figure 3.

Downloaded from https://academic.oup.com/icesjms/article-abstract/65/3/379/784056
by Old Dominion University user
on 15 May 2018

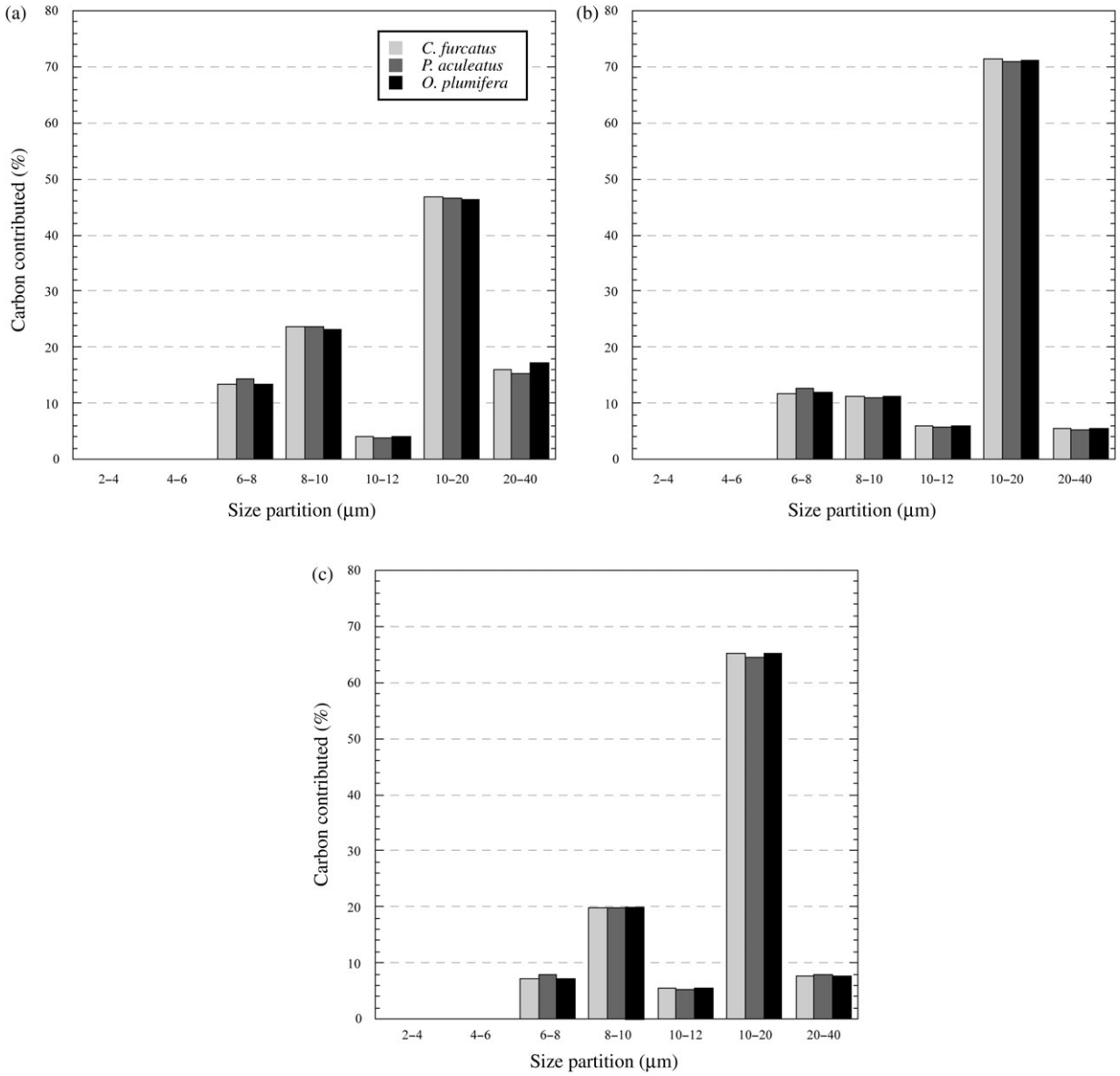

Figure 7. Percentage of simulated total carbon uptake provided to each copepod species by cells within seven size partitions for (a) prey spectrum 1, (b) prey spectrum 2, and (c) prey spectrum 3. The standard spectrum (4) case is shown in Figure 5d. The mature female preference curve (d_P = 40 μm) and standard value for U_D (0.2 mm s^{-1}) were used. Details regarding the size partitions are as described for Figure 5.

prey density required to achieve basal needs relative to the simulations with standard forage conditions (Figure 3j–l). Along with the higher rates of carbon uptake, the shift towards larger prey in spectra 2 and 3, combined with the adult copepod size preference, leads to $I{:}Z_M$ ratios (and therefore ingestion rates) that are ~2.5 times greater than when spectra 1 or 4 are applied (Figure 6i–l). Also, there is little discernible difference in this ratio or the ingestion rates of the three species when these two spectra are applied. The primary difference in size-partitioned carbon contribution between spectra 2 and 3 and the standard prey distribution (spectrum 4) lies in the contribution of 10–20 μm prey (65–72% vs. 52%; Figures 5d and 7b and c).

Prey spectrum 3 results in the largest percentage contribution to total carbon uptake (20%) by the 8–10 μm partition (compare Figure 7c with Figures 5d and 7b). The highest contribution from the 20–40 μm partition occurs when spectrum 4 is applied, although this partition is more prominently represented within spectrum 3 (Figure 2). Total carbon uptake is lowest when spectrum 4 is applied (Figures 3j–l and 6d–i), despite having the strongest relative contribution by large cells to the mature females' diet. Thus, the overall make-up of the prey field (i.e. how prey is distributed over size class) contributes to the relative success of copepod foraging.

Dependence of copepodites on distribution of prey size

Copepodite preference for small prey (Figure 1) results in a reduction in carbon uptake for spectrum 1 compared with spectrum 4 of ~20% for *P. aculeatus* (Figure 3b vs. Figure 8b) and <10% for the other two species (Figures 3a and c vs. 8a and c). Thus, compared with spectrum 4, the shift towards smaller prey

Downloaded from https://academic.oup.com/icesjms/article-abstract/65/3/379/784056
by Old Dominion University user
on 15 May 2018

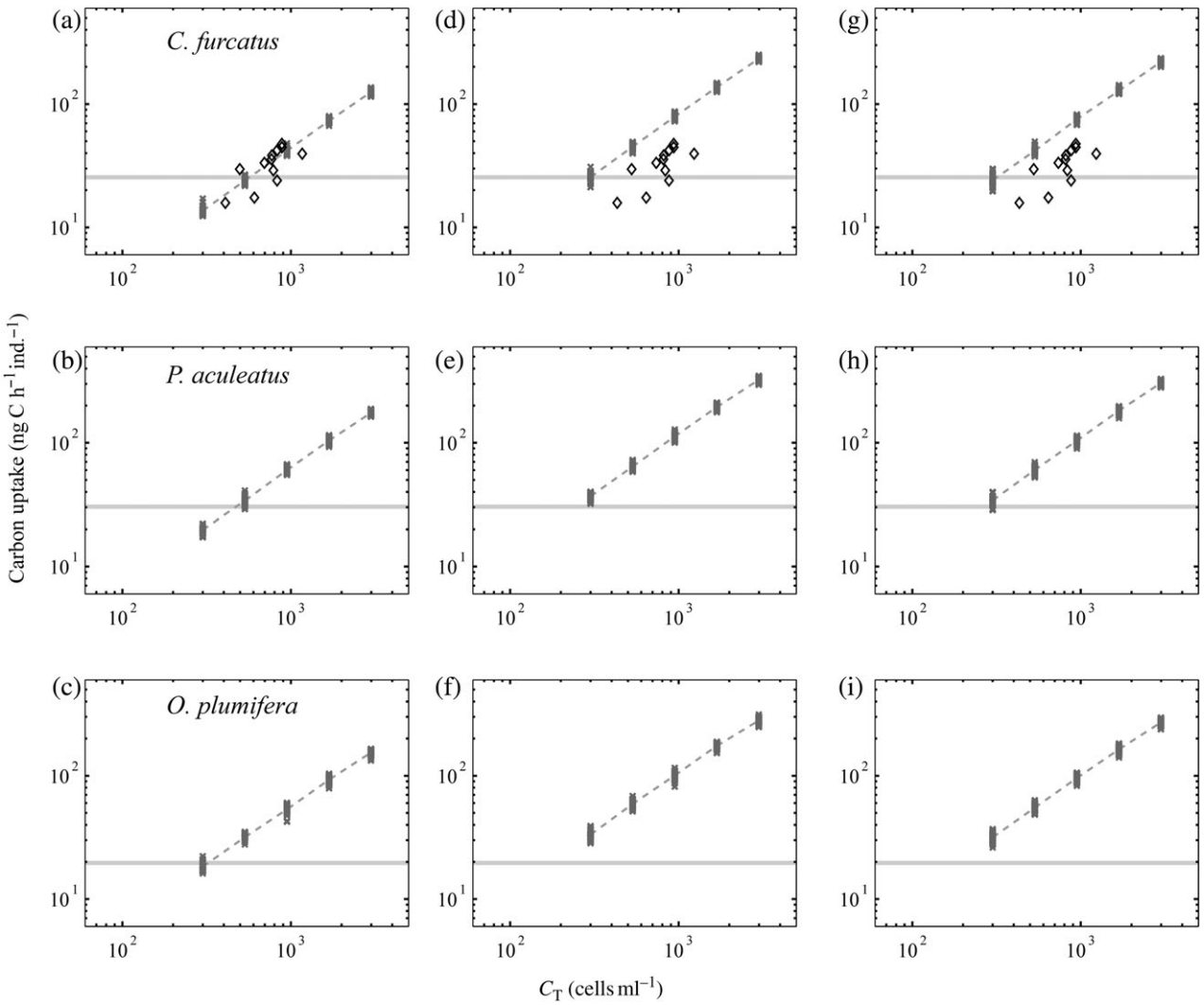

Figure 8. Simulated carbon uptake (ng C h^{-1} ind.$^{-1}$) as a function of total cell concentration (C_T) for the youngest copepodites (d_P = 10 μm) for (a–c) prey spectrum 1, (d–f) prey spectrum 2, and (g–i) prey spectrum 3. The standard value for U_D (0.2 mm s^{-1}) was used. Corresponding results for the standard prey distribution (spectrum 4) are shown in Figure 3a–c. Other details are as described for Figure 3.

in spectrum 1 exerts much less impact on the grazing success of the copepodites than on the mature females (Figure 6a–c). Furthermore, with this prey spectrum, all three species meet their minimal metabolic needs at a prey concentration of less than 550 cells ml^{-1} (Figure 8a–c), a density of small cells that is maintained even in the surface summertime mixed layer of oligotrophic subtropical waters (see Figure 3 in Paffenhöfer *et al.*, 2003). The percentage of carbon contributed by the different prey-size partitions demonstrates that, in relation to spectrum 4 (Figure 5a), the 10–20 μm prey contribution is reduced from 30% to 20%. This reduction is compensated for by prey within the 2–6 μm partition that provides more than 50% of the total carbon acquired when spectrum 1 is applied (Figure 9a). Grazing by the copepodite stages on a prey field dominated by the smallest size classes (spectrum 1) is the only instance where the 10–20 μm size class does not rank as the single largest contributor to total carbon uptake (Figures 5, 7, and 9).

When prey spectra 2 and 3 are applied, all three species achieve basal needs at the minimum prey concentration (300 cells ml^{-1}, Figure 8d–i). The availability of larger cells within these prey distributions provides some advantage in the grazing success of the copepodites, but it is considerably reduced relative to that of the adult females. Nevertheless, for spectra 2 and 3, the 10–20 μm prey partition remains dominant. In both cases, this partition contributes ~45% to the overall carbon uptake (Figure 9b and c), though this is a significant reduction from the 65–72% contribution that was evident for the mature copepods (Figure 7b and c). The relative differences in dominant prey partitions over the 4–10 μm cells (Figure 2) are more directly reflected in the percentage carbon distributions than was true for the adult female simulations, with spectrum 2 exhibiting a more pronounced contribution at 4–8 μm, and spectrum 3 featuring the 8–10 μm partition (Figure 9b and c).

Simulation group 3: effect of turbulence on predator–preyen counter rate and grazing success

Theoretical encounter rates (Z_A)

Theoretical rates of predator–prey encounter (Z_A, Table 2) were calculated using Equation (4) to establish a baseline for comparison with the variable turbulence simulations. For a given

Downloaded from https://academic.oup.com/icesjms/article-abstract/65/3/379/784056
by Old Dominion University user
on 15 May 2018

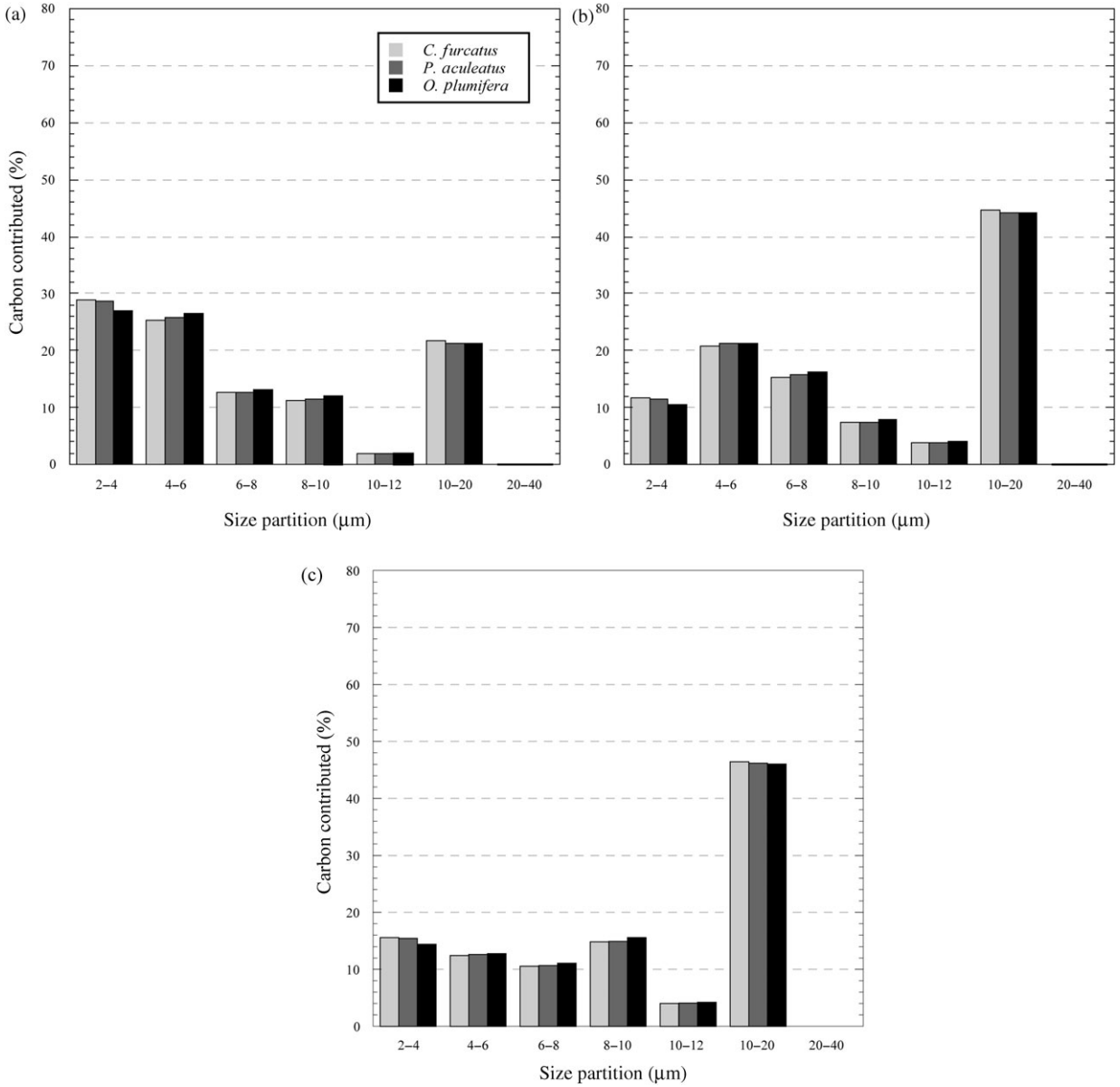

Figure 9. Percentage of simulated total carbon uptake provided to each copepod species by cells within seven size partitions for (a) prey spectrum 1, (b) prey spectrum 2, and (c) prey spectrum 3. Results obtained for the standard prey distribution (prey spectrum 4) are shown in Figure 5a. The youngest copepodite preference curve (d_P = 10 μm) and value for U_D (0.2 mm s^{-1}) were used. Details regarding the size partitions are consistent with Figure 5.

turbulence intensity, prey-partition-specific values of the theoretical encounter rate for each copepod species demonstrate that Z_A varies with the different prey densities of each size class (C_P) and the associated velocities (U_P). This prey velocity combines sinking speed (w_s under the heading "Impact of turbulence") with the individual velocities of motile prey. For the smallest size partition and no turbulence ($|\overrightarrow{u}_D| = 0.0$ mm s^{-1}), Z_A differs by more than two orders of magnitude between species. *Oithona plumifera* exhibits a similar variation in the magnitude of Z_A between the two turbulence intensity conditions. The most mobile species (*C. furcatus*) derives the least enhancement to encounter rate in turbulence waters ($|\overrightarrow{u}_D| = 6.5$ mm s^{-1}). Over the three species of copepod, it is apparent that this turbulence-derived enhancement in encounter rate varies inversely with each predator's characteristic ambit speed (U_C).

Variation of Z_A with prey partition and turbulence intensity reveals that *C. furcatus* has the lowest overall range in Z_A (Figure 10a). The gradient in Z_A at low turbulence intensities is significantly sharper for *P. aculeatus* and in particular for *O. plumifera* (Figure 10b and c). All three species exhibit either a plateau or a local maximum in Z_A associated with the 10–20 μm size class (Figure 10, size partition 5), which results from the lower number of cells in the 20–40 μm partition and the comparable population of the narrow 8–10 μm partition that has lower U_P. The predominance of smaller prey results in the 2–4 μm partition consistently exhibiting the maximum values of Z_A, which are more

Downloaded from https://academic.oup.com/icesjms/article-abstract/65/3/379/784056
by Old Dominion University user
on 15 May 2018

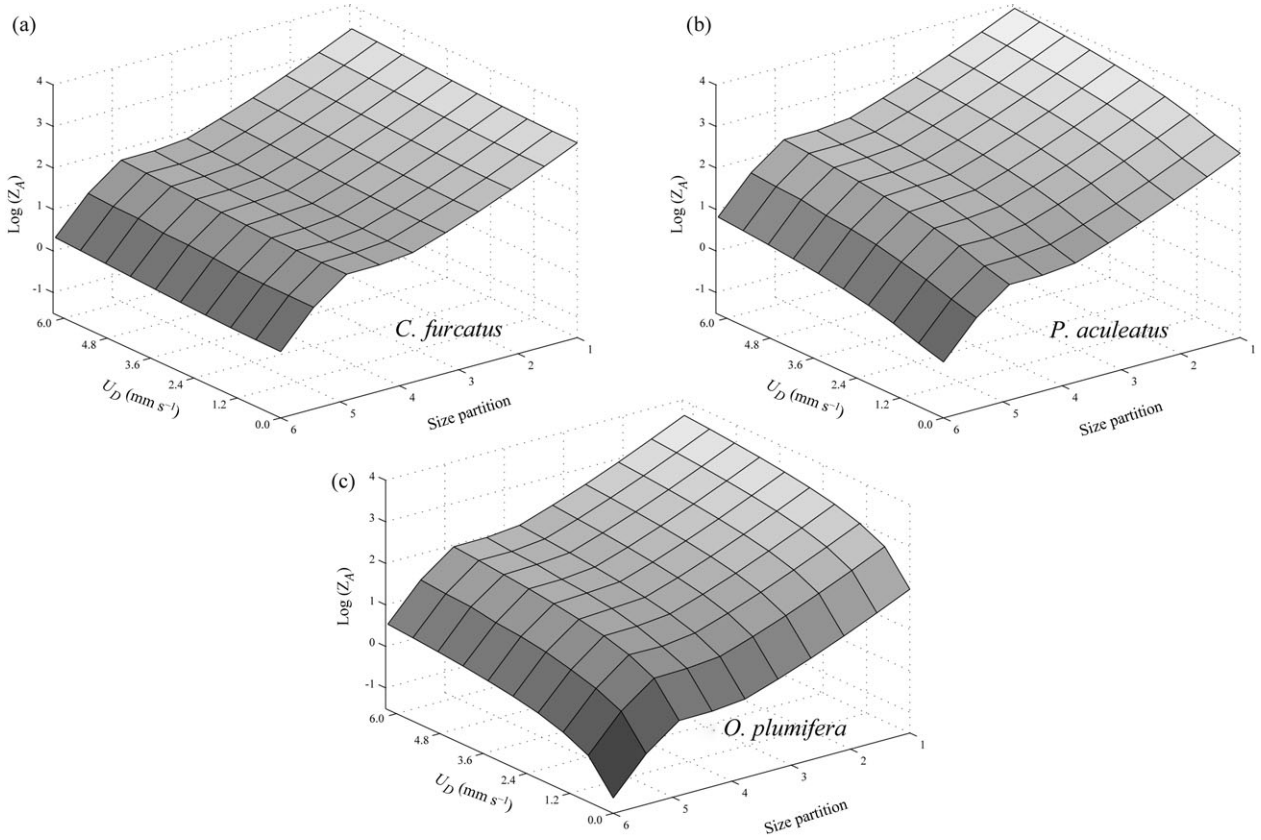

Figure 10. Theoretical encounter rate (Z_A, cells h^{-1} ind.$^{-1}$) as it varies with turbulence intensity and size partition for (a) *C. furcatus*, (b) *P. aculeatus*, and (c) *O. plumifera*. Z_A is determined with Equation (4). Further details of this calculation and the appropriate values are given in the text and Table 2. The shading indicates the magnitude of Z_A for a given set of conditions, with darker shading corresponding to higher encounter rates. The six partition indices are (1) 2–4 μm, (2) 4–6 μm, (3) 6–8 μm, (4) 8–10 μm, (5) 10–20 μm, and (6) 20–40 μm.

than 1.5 orders of magnitude greater than those for the 10–20 μm partition.

Simulated encounter rates (Z_M)

For each copepod species, the impact of turbulence intensity on encounter rates increases with increasing cell concentration (Figure 11a–c). Encounter rates for *C. furcatus* are somewhat reduced at the highest turbulence intensities, whereas *P. aculeatus* reveals no trend and *O. plumifera* exhibits an increase of ∼70% (Figure 11a–c). The ingestion-to-encounter-rate ratios (I:Z_M) at all three prey concentrations demonstrate that the youngest copepodites consume essentially all encountered cells, especially at the lowest prey density (Figure 11d–f). However, although this ratio remains essentially 1 for *C. furcatus* as prey concentration increases, both *P. aculeatus* and *O. plumifera* exhibit a clear reduction, and values of 0.9–0.95 are obtained when C_T = 950 cells ml^{-1} (Figure 11e and f). When U_D exceeds 1 mm s^{-1}, Z_M for *O. plumifera* exhibits an increased slope that is most pronounced at the highest prey concentration (Figure 11c) and is reflected in I:Z_M (Figure 11f). For the other two species, I:Z_M exhibits no dependence on U_D at a given prey concentration (Figure 11d and e). Maximal Z_M for *C. furcatus* is slightly below 4 × 10^3 cells h^{-1} ind.$^{-1}$, whereas that for *P. aculeatus* and *O. plumifera* slightly exceeds this value. In conjunction with the downward shift in the ingestion-to-encounter-rate ratio exhibited for the latter species, a threshold for encounter rate of ∼1 cell s^{-1} is indicated. Further, the downward trend apparent in this ratio at the higher turbulence intensities for *O. plumifera* suggests that this is biomechanical in nature and does not derive from short-term satiation.

By integrating Z_A (Figure 10) over size partition, direct comparison can be made between the simulated and theoretically derived rates (Figure 11a–c). For the two faster moving predators, Z_A is constant at lower values of U_D, then begins to increase monotonically above a threshold in turbulence intensity (Figure 11a and b). This break in the Z_A curves occurs at ∼30% of the typical predator velocity. For *O. plumifera*, Z_A consistently increases but is less than Z_M until U_D exceeds 3 mm s^{-1} (Figure 11c). Thus, the theoretical encounter rates reveal a transition between behaviourally controlled rates of predator–prey encounter and rates controlled by fluid turbulence.

For *C. furcatus*, as U_D exceeds 1 mm s^{-1}, Z_A increases while Z_M trends downwards (Figure 11a). At the lower turbulence intensities where the theoretical rates are constant for *C. furcatus*, these compare most favourably with the modelled rates when C_T = 534 cells ml^{-1}. For *P. aculeatus*, the theoretical and modelled encounter rates (C_T = 300 cells ml^{-1}) exhibit excellent agreement for U_D below 2 mm s^{-1}. The theoretical result approaches 10^4 cells h^{-1} ind.$^{-1}$ at maximum U_D, although even at a prey concentration of 950 cells ml^{-1}, the modelled encounter rates remain below 5 × 10^3 cells h^{-1} ind.$^{-1}$ (Figure 11b). However at the two highest prey concentrations (1700 and 3000 cells ml^{-1}), Z_M for youngest copepodites exceeds 10^4 cells h^{-1} ind.$^{-1}$ at standard

Downloaded from https://academic.oup.com/icesjms/article-abstract/65/3/379/784056
by Old Dominion University user
on 15 May 2018

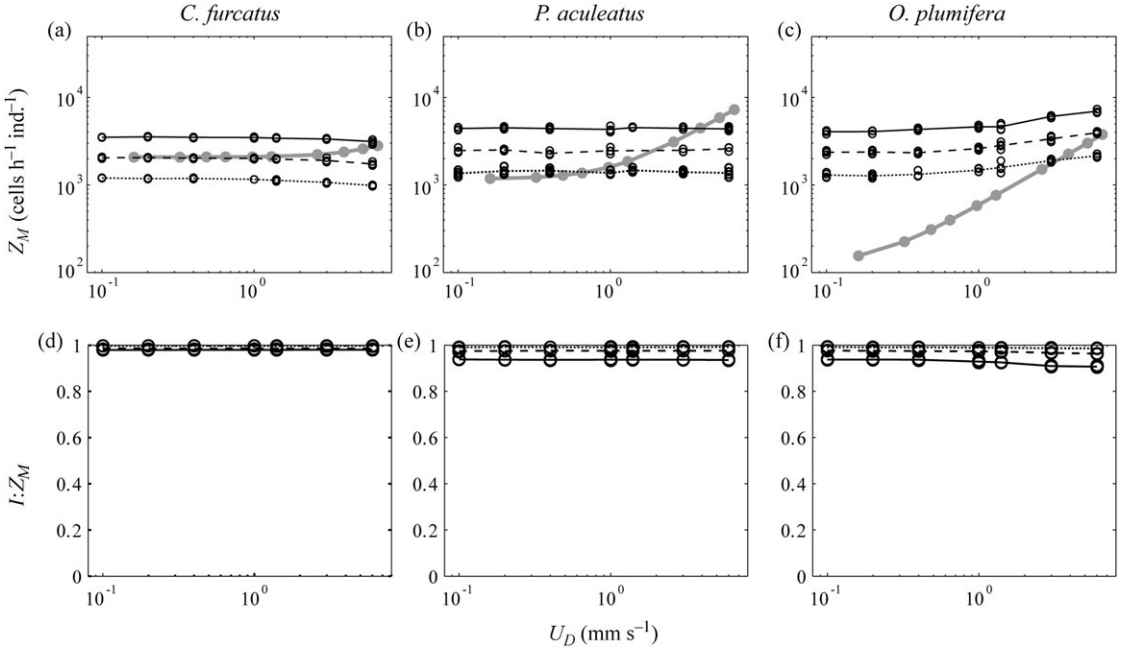

Figure 11. Simulated cell-encounter rate (Z_M, cells h^{-1} ind.$^{-1}$) and I:Z_M (dimensionless) as a function of turbulence velocity (U_D) for *C. furcatus* (left column); *P. aculeatus* (middle column); and *O. plumifera* (right column). Total cell concentrations (C_T) of 300 cells ml^{-1} (dotted line), 534 cells ml^{-1} (dashed line), and 950 cells ml^{-1} (solid line) were used. For each species, the theoretical encounter rates obtained from Equation (4) and integrating across size partition are also shown (panels a–c, heavy grey line with filled circles).

U_D (Figure 4b). For *O. plumifera*, Z_A agrees well with Z_M at only the highest values of U_D and is an order of magnitude lower than Z_M in quiescent or reduced intensity regimes (Figure 11c).

Effect of turbulence intensity on carbon uptake

Carbon uptake dependence on turbulence intensity for the copepodites and mature females (Figure 12) exhibits the same general decrease as size preference shifts towards larger prey that was noted earlier (Figure 3). Increasing U_D gives the same general carbon uptake trends as obtained for the encounter rates for each species (Figure 11a–c). *Clausocalanus furcatus* exhibits a consistent decrease in uptake that is most pronounced at the higher turbulence intensities (Figure 12a and d); *P. aculeatus* exhibits little discernible trend (Figure 12b and e); and *O. plumifera* exhibits increasing carbon uptake especially for U_D above 1 mm s^{-1} (Figure 12c and f). Independent of turbulence level, *C. furcatus* (Figure 12a and d) and *P. aculeatus* (Figure 12b and e) are unable to achieve basal requirements at the lowest prey density (C_T = 300 cells ml^{-1}). Mean carbon uptake for the copepodite stage of *O. plumifera* is just below basal rates at low U_D and surpasses this threshold when U_D exceeds 1 mm s^{-1} (Figure 12c). For the most energetic turbulence regime, mean uptake for mature females is just below the basal rate (Figure 12f).

Carbon uptake as a function of prey size and turbulence velocity differs for the three species and for the prey-size preferences exhibited by copepodites (Figure 13a–c) and mature females (Figure 13d–f). Consistent with the results described for the size preference simulations (Figure 5a, under the "Results" heading), the largest size partition is eliminated as a nutritional source when d_P = 10 μm (Figure 13a–c). For *C. furcatus*, prey in the 10–20 μm partition make the greatest contribution to overall uptake, followed by prey in the 2–4 μm partition (Figure 13a). Total carbon uptake is reduced systematically with increasing

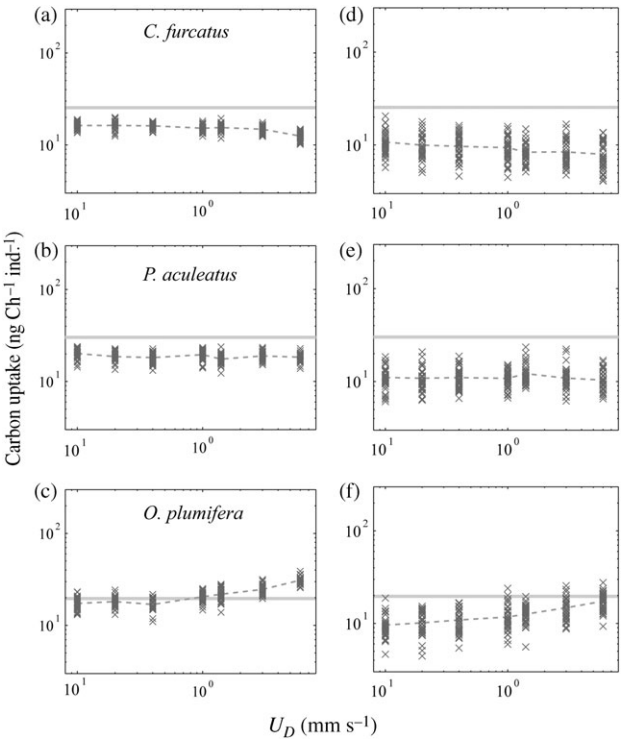

Figure 12. Effect of turbulence intensity on simulated total carbon uptake rate with C_T = 300 cells ml^{-1} for (a–c) copepodites (d_P = 10 μm), and (d–f) mature females (d_P = 40 μm). The standard prey distribution (prey spectrum 4, Table 1) was used. The individual simulated rates (cross) and the mean rate as a function of U_D (dashed line) are shown. Basal metabolism (grey horizontal line) is as described for Figure 3.

Downloaded from https://academic.oup.com/icesjms/article-abstract/65/3/379/784056
by Old Dominion University user
on 15 May 2018

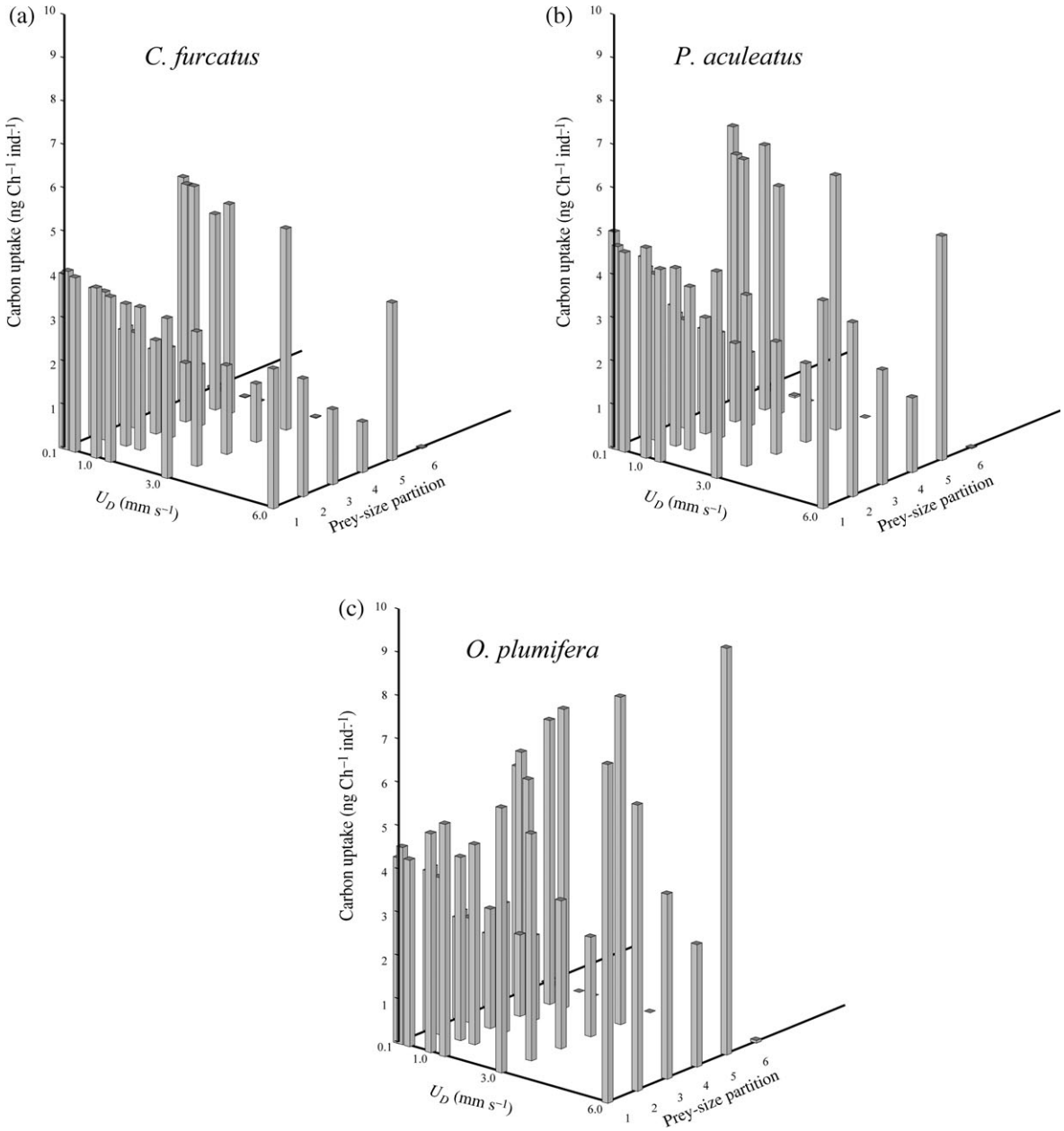

Figure 13. Effect of turbulence intensity on size-partitioned simulated carbon uptake when $C_T = 300$ cells ml^{-1} for (a and d) *C. furcatus*, (b and e) *P. aculeatus*, and (c and f) *O. plumifera*. Panels a–c are for copepodites ($d_P = 10$ μm), whereas panels (d–f) show results for mature females ($d_P = 40$ μm). The six partition indices are (1) 2–4 μm, (2) 4–6 μm, (3) 6–8 μm, (4) 8–10 μm, (5) 10–20 μm, and (6) 20–40 μm. Note that panels (d)–(f) are reproduced on the next page.

turbulence for all of the individual size partitions (Figure 13a) and is most pronounced for the 10–20 μm partition. At maximum U_D, the carbon derived from cells in the 2–4 μm partition is nearly equivalent to that in the 10–20 μm partition and is followed closely by prey in the 4–6 μm partition. For *P. aculeatus*, carbon derived from prey in the largest size partitions decreases with intensifying turbulence (Figure 13b). The total uptake for this species demonstrated no clear trend with turbulence intensity (Figure 12b), and compensation for the reduced carbon contribution derived from large prey is achieved through the smaller size classes (Figure 13b). For *O. plumifera*, as turbulence intensifies, carbon uptake increases across all partitions with no obvious modification to their relative contribution (Figure 13c).

Again consistent with the preference-curve simulations (Figure 5d), prey with ESD <6 μm makes no nutritional contribution to the adult copepod diet (Figure 13d–f). For *C. furcatus*, the negative impact of turbulence intensity appears primarily as reduced uptake within the 10–20 μm partition (Figure 13d). For the two active smaller size partitions, the contribution to carbon uptake remains relatively constant, which indicates that successful perception is the primary factor limiting consumption. The uptake contribution of the 20–40 μm partition demonstrates a consistent

Downloaded from https://academic.oup.com/icesjms/article-abstract/65/3/379/784056
by Old Dominion University user
on 15 May 2018

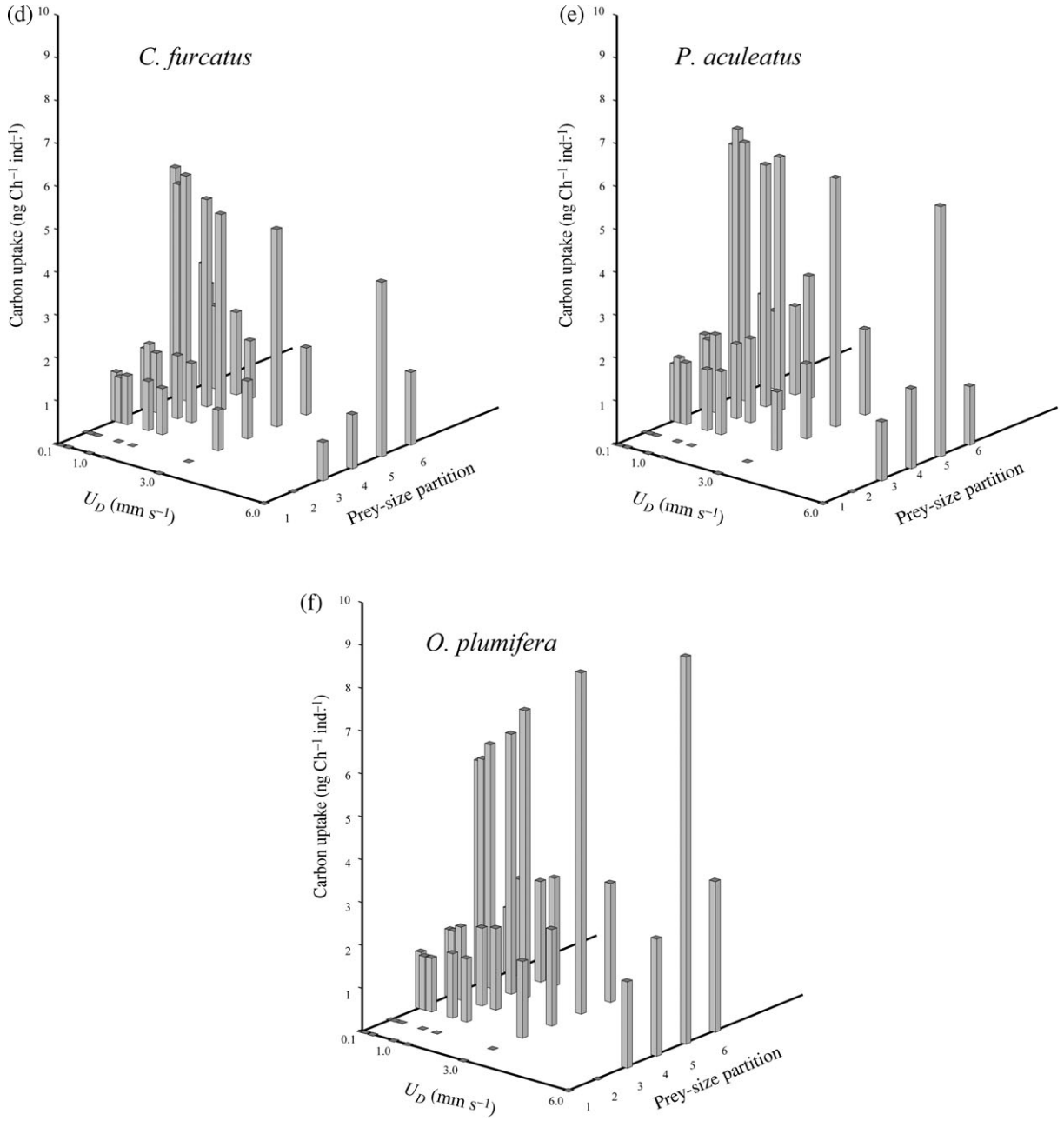

Figure 13. *Continued*

decrease from minimal U_D through 1.0 mm s^{-1}. At higher U_D, no clear trend in the realized contribution to carbon uptake is apparent, reflecting the greater stochasticity associated with encountering the relatively scarce large prey. For *P. aculeatus*, there is again no clear trend associated with increasing turbulence intensity (Figure 12e). In contrast to the copepodite simulation, no definitive trend in carbon contributed by the 10–20 μm partition appears. However, the upward shift in total carbon uptake apparent for $U_D = 1.4$ mm s^{-1} (Figure 12e) primarily reflects an increased contribution from the 20–40 μm prey partition (Figure 13e), which emphasizes the stochasticity associated with capturing cells in this size class. Finally, for *O. plumifera*, all four of the contributing partitions exhibit increased rates of carbon uptake with more intense turbulence (Figure 13f).

Discussion

Grazing-rate modification by prey-selection shifts that accompany copepod maturation

The prey-size preference simulations provided some general insights into how ingestion rates differed with developmental stage. Carbon uptake decreased with stage, which is consistent with the documented decrease in metabolism per unit body weight (QO_2) as an individual matures (Epp and Lewis, 1980). The simulated carbon uptake rates became more variable as dependence on larger, less abundant prey increased. Additionally, for a given prey concentration (C_T, cells ml^{-1}), cell ingestion rates (I, cells h^{-1} ind.$^{-1}$) changed by more than an order of magnitude from the copepodite stage to the mature

Downloaded from https://academic.oup.com/icesjms/article-abstract/65/3/379/784056
by Old Dominion University user
on 15 May 2018

females with a corresponding reduction of ~65 ng C h^{-1} ind.$^{-1}$ (~35%) in carbon uptake. Along with this reduced uptake, nutritional contributions from cells with ESD <6 μm were minimized, whereas the percentage contribution of the 10–20 μm partition increased from ~35% to 53% and the 20–40 μm partition increased from 0% to ~18%. These model results are consistent with growth coefficients determined for natural copepod populations that decreased with advancing life stage (see Table 7 in Webber and Roff, 1995a) and offshore phytoplankton populations dominated by picoplankton that are less accessible to the more advanced developmental stages (note Figure 3 in Webber and Roff, 1995b).

For the three more advanced developmental stages, $I{:}Z_M$ (i.e. prey selectivity) was constant with C_T and consistently decreased with maturation. Thus, the shift in size preference that accompanies maturation led to reduced ingestion and carbon uptake. The simulation results suggested that short periods of satiation occur, which temporarily halt prey acquisition. These episodes were related to consumption of a large cell with high carbon content. For the copepodites, essentially all encountered cells were consumed at low C_T. At higher concentrations, the ratio of ingestion-to-encounter rate decreased, suggesting a practical limit to cell acquisition associated with biomechanical limitations.

Influence of prey spectrum on vertical distribution of copepod developmental stage

With its predominance of small cells, spectrum 1 best represents oligotrophic, upper ocean conditions. With this food distribution, mature females required a 35–55% higher prey concentration to meet basal metabolic needs, with *O. plumifera* requiring the greatest increase. *Clausocalanus furcatus* and *P. aculeatus* required $C_T > 10^3$ cells ml^{-1} to meet their minimum metabolic needs. In the observed planktonic spectra that consisted of four profiles with five or sixth depths (15–140 m), there were five instances where such cell densities were observed (see Figure 2 in Paffenhöfer *et al.*, 2003). Of these, all were associated with the DCM except for one occurrence within the surface mixed layer. For all the observed profiles, C_T decreased monotonically with depth until the DCM was reached. Thus, with regard to dietary needs, mature female copepods are better situated near the DCM.

Prey spectrum 1 resulted in simulated carbon uptake rates derived from the 8–10 μm partition that are 50% higher despite a cell population within this partition that is identical with that of spectrum 4. This resulted from the lower large cell component of spectrum 1. For spectra 2 and 3, which emphasize larger prey, the mature females generally met basal requirements when C_T was 500 cells ml^{-1}, and always did so at higher concentrations. Additionally, more than 60% of their carbon uptake was derived from the more prominent population of 10–20 μm cells that these two spectra feature. Comparison of the simulated total carbon uptake obtained using these four spectra revealed a direct relationship with the 10–20 μm prey-size partition. In the Sargasso Sea profiles, this partition typically accounted for 25–50% of the total volume of planktonic cells (2–20 μm in size; see Figure 9 in Paffenhöfer *et al.*, 2003). This reinforces the conclusion that the most suitable ecological niche for mature females occurs deeper in the water column where larger prey are more prevalent.

Prey spectrum 1 allowed the youngest copepodite stage of all three species to meet basal needs at or below 550 cells ml^{-1}. When compared with spectrum 4 (standard case), simulated carbon uptake was somewhat reduced (10–20%), with *P. aculeatus* exhibiting the greatest decrease. The most prominently reduced portions of the prey population between spectrum 4 and spectrum 1 were the 10–20 μm partition and to a lesser degree the 6–8 μm partition. Thus, the youngest developmental stage was also influenced by the 10–20 μm partition. However, cells ≤6 μm ESD contribute more than 50% of the consumed carbon, and both of the two smallest size partitions individually contribute more to the copepodite diet than the 10–20 μm partition, which provided only ~20% of the total. Prey spectra 2 or 3 also allowed the youngest copepodites to meet basal needs (on average) at the lowest prey concentration, and the 10–20 μm partition was again the dominant nutritional source, though its contribution dropped to ~42% compared with the more than 60% contribution made to the adult female diet.

Regardless of prey-size distribution, the copepodites for all species meet nutritional needs for $C_T \leq 550$ cells ml^{-1}. Measurements from the Sargasso Sea (Paffenhöfer *et al.*, 2003) proved that more than 90% of the observed cell concentrations exceeded 640 cells ml^{-1} (data not shown), which ensures that immature individuals will have sufficient food. Moreover, the combination of spectra 1 and the youngest copepodite stage was the only simulation for which the 10–20 μm partition did not make the largest individual dietary contribution. This suggests that, for immature individuals, a near-surface niche exists that is less accessible for mature females. Thus, the simulations support the conclusion that the specific make-up of the prey field contributes to where various copepod developmental stages can exist. This result is consistent with natural distributions that exhibit such a vertical stratification of copepod life stages (Fragopoulu *et al.*, 2001) and vertical copepod speciation that is associated with water-column-density structure and DCM location (Ambler and Miller, 1987; Peralba and Mazzocchi, 2004; Ramfos *et al.*, 2006). Other analyses of *in situ* observations of vertical copepod distributions have addressed the possibility that their peak abundance coincides with the maximal rate of primary productivity, which is generally 5–10 m above the DCM (Napp *et al.*, 1988; Herman, 1989). In this model, the prey population is static, which does not allow differentiation of copepod response to distinct peaks in prey biomass or growth rate within these simulations.

Varying impact of turbulence intensity on grazing success across copepod species

The divergence of the theoretically derived encounter rate from the modelled rate (Z_M at 300 cells ml^{-1}) reflected a threshold in turbulence intensity that related directly to the magnitude of each predator's characteristic sampling velocity below which the explicit foraging behaviour dominates (Figure 11a–c). The theoretical encounter rate Z_A [cells h^{-1} ind.$^{-1}$, Equation (4)] depended solely on geometrical constraints and did not account for prey removal. Cells in the 10–20 μm partition accounted for only ~1–4% of the total prey population (Table 1), so although they may contribute significantly to carbon uptake because of their volume, they exerted little influence on Z_M (cells h^{-1} ind.$^{-1}$).

For *C. furcatus*, there were two differences between the modelled and theoretical encounter rates. First, Z_M for C_T = 300 cells ml^{-1} was always lower than Z_A. Second, Z_A increased with turbulence intensity above $U_D = 1.0$ mm s^{-1}, whereas Z_M for all three prey concentrations decreased at the highest turbulence intensities. This second distinction derives from the cell

Downloaded from https://academic.oup.com/icesjms/article-abstract/65/3/379/784056
by Old Dominion University user
on 15 May 2018

removal that was tracked in the simulations and suggested that this species can very effectively clear a given water parcel. Such a localized reduction in prey concentration would diffuse more effectively into surrounding waters as turbulence intensity increases resulting in a more extensive region with reduced prey concentration. Thus, this foraging method may be quite effective at clearing a given water parcel; however, this technique is potentially prone to self-induced grazing limitation via generation of localized patchiness in the prey population if shifting to a new location is not employed frequently enough. In nature, it is likely that species that employ foraging methods similar to *C. furcatus* will respond to prey gradients in a manner that minimizes this potential limitation, and models that incorporate such search strategies have been developed (Leising, 2001).

For all developmental stages of *C. furcatus*, an increase in turbulence intensity resulted in reduced total carbon uptake caused by a disproportionate reduction in the contribution obtained from the 10–20 μm partition (Figure 13a and d). At low U_D [mm s^{-1}, Equation (3)], this partition was clearly the dominant nutritional source; however, at maximum U_D, it was notably reduced and, for the youngest copepodites, was equivalent to the contribution derived from the 2–4 μm partition. This result is consistent with Wiggert *et al.* (2005), where it was determined that this species had a relative disadvantage in acquiring large, non-motile prey (ESD $>$ 40 μm). Higher sinking velocities of the larger cells produced elevated, orthogonal relative velocities between *C. furcatus* and its prey, which reduced the likelihood of capture. With prey ESD capped at 40 μm in this study, this species-dependent dietary distinction was no longer apparent at standard U_D (Figure 5). However, as turbulence intensity increased, the associated decrease in carbon uptake derived from the 10–20 μm size class by all developmental stages suggests another interaction between behaviour and environmental conditions for this species. Because the turbulence velocity of each cell (prey) is stochastic, the directional vectors of prey and predator are not necessarily orthogonal, as can be assumed for gravitationally driven sinking velocities and the typical sampling plane of *C. furcatus* that is at least quasi-horizontal (cf. Figure 1 of Mazzocchi and Paffenhöfer, 1999). The simulated AOP of this species is a long, narrow cone. The clear dependence on U_D for uptake of 10–20 μm ESD cells suggested that, as their relative velocities increased, the angular range of oblique predator–prey directional vectors likely to result in cell acquisition narrowed.

For *P. aculeatus*, Z_A and Z_M matched at lower values of U_D and again diverged at higher turbulence intensities. In contrast to the results noted above for *C. furcatus*, Z_M exhibited no dependence on U_D for this species. Thus, the foraging mechanism of *P. aculeatus* was less prone to inducing self-limitation, because repeated sampling of a given water parcel did not occur. The total carbon uptake curves also exhibited no clear trend as U_D increased for either developmental stage (Figure 12b and e). As turbulence intensity increased, copepodites derived less carbon from the 10–20 μm partition. This reduction was compensated for by additional carbon uptake derived from smaller prey (Figure 13b).

The strongest deviation between the theoretical and simulated encounter rates was exhibited by *O. plumifera*, with Z_A at the least energetic turbulence condition ($U_D = 0.17$ mm s^{-1}), being an order of magnitude lower than Z_M (Figure 11c). Although Z_M exhibited a plateau at low turbulence intensity similar to that of the other two species, Z_A increased monotonically over the applied range of turbulence intensities. These differences yielded the most prominent example of the contribution that foraging behaviour makes towards facilitating grazing success. Indeed, these results suggested that the frequent, oblique upward jumps employed by *O. plumifera* significantly mitigate the extremely low encounter rates predicted by the theoretical relation by allowing for effective sampling of the water column through frequent insertion into a completely new parcel of water with a fresh group of potential prey. Carbon uptake for *O. plumifera* had a clearly positive impact by increasing turbulence intensity that manifests across all contributing size partitions and developmental stages (Figure 13c and f).

Each species exhibits a unique response to increasing turbulence whereby the encounter rate decreased, remained constant, or increased. These responses relate inversely to the characteristic ambit velocity and reflect the dome-shaped relation in predator–prey encounter with increasing turbulence kinetic energy (TKE) reported in the literature (Mackenzie *et al.*, 1994; Jenkinson, 1995). A reduced encounter rate at higher TKE reflects time spent on pursuit, handling of prey, or temporary satiation (Mackenzie *et al.*, 1994; Metcalfe *et al.*, 2004). The varying impact of turbulence exhibited in the simulations presented here also suggests that spatial heterogeneity in copepod speciation will develop, with *Oithona* preferring regions prone to stronger mixing (e.g. the surface mixed layer) and *Clausocalanus* favouring more stable fluid regimes. Although there is observational evidence for vertical structure in metazoan distribution associated with turbulence, determination of clear relationships and species tendencies remains elusive and often contradictory (Haury *et al.*, 1990; Incze *et al.*, 2001; Maar *et al.*, 2006).

Conclusions and future prospects

The model results presented here demonstrate differential response to variation in environmental conditions by three common copepod species that employ distinct methods of grazing. This differential response extends through the range of developmental stages included in these simulations. The coincident persistence and spatial distribution of these copepod species, and their developmental stages, depend not only on prey concentration but are also controlled by the make-up of the prey field (i.e. how prey is distributed over size class). The results presented here suggest a naturally occurring niche distribution that promotes the near-surface presence of younger copepodites over the mature females. A similar impact on vertical distribution of species in response to varying turbulence intensity is indicated. Thus, preferred niches may exist that would lead to spatial heterogeneity if the underlying environmental conditions persisted. Given that the oceanic environment is typically subject to contemporaneous disequilibrium, the integrative effect results in collective persistence of species.

A primary motivation for the development of this Lagrangian IBM is to develop approaches for including species-specific meta- and mesozooplankton grazing into models designed to investigate large spatial scales and seasonal to interannual timescales. For such broad scale applications, a fundamental interest is to advance the capacity to predict how marine ecosystems and oceanic biogeochemical cycling will respond to natural and anthropogenically driven changes in global climate. For example, if climate change resulted in increased stratification and modified intensity of small-scale oceanic turbulence, the simulation results presented here suggest that *Clausocalanus* would do well in a less energetic turbulent regime which may then enhance biogenic

Downloaded from https://academic.oup.com/icesjms/article-abstract/65/3/379/784056
by Old Dominion University user
on 15 May 2018

export to the deep ocean. However, if climate change leads to higher windspeeds (e.g. Goés *et al*., 2005), the accompanying increase in the intensity of upper ocean turbulence would favour *Oithona*. In that case, it could be argued that export fluxes would decrease because this species employs coprophagy and produces smaller, slower sinking faecal pellets that promote upper ocean retention of organic matter via bacterial remineralization (González *et al*., 2000; Svensen and Nejstgaard, 2003; Huskin *et al*., 2004). However, whether ambush predators such as *Oithona* have a preference for higher levels of turbulence remains to be determined (Kiørboe and Saiz, 1995; Visser and Stips, 2002).

Development of zooplankton IBMs with a rule set sufficient to generate robust emergent behaviour that can provide parameterizations for larger scale models requires comprehensively characterizing motile prey behaviour and determining how copepod foraging ambits and prey perception are influenced by non-organic particulates (e.g. silt), salinity, density gradients, and velocity shear (Paffenhöfer, 1972; Wiggert *et al*., 2005; Woodson *et al*., 2005; Seuront, 2006). Also, process studies that characterize typical foraging behaviours and full accounting of metabolic costs incurred by the various grazing methodologies (e.g. through determination of oxygen utilization) are critical needs. Such studies, combined with the development of zooplankton IBMs that include realistic representation of environmental conditions, will allow development of parameterizations that account for the full diversity of copepod foraging behaviours in response to environmental perturbations. This approach is analogous to that now being used by marine ecosystem modellers to incorporate the myriad planktonic behaviours within a tractable set of functional groups (Legendre and Michaud, 1998; Hood *et al*., 2006). If this could be accomplished, then a zooplankton-based counterpart to a recent effort—wherein a realistic distribution of ecotypes (i.e. phytoplankton groupings) emerged naturally from an initial superset based on the prevailing light field, nutrient availability, and water column structure within a global general circulation model (Follows *et al*., 2007)—could be developed. What is especially appealing about such an application is the possibility it provides for using the inherently synthetic nature of a model to explore global-change scenarios and how planktonic community structure is likely to adjust or even possibly facilitate systemic response that mitigates climate change.

Acknowledgements

The National Oceanographic Partnership Program supported this research (Grant # N00 014-02-1-0370). G-A.P was supported by the National Science Foundation (OCE-9911513, towards an understanding of the existence of small oceanic planktonic copepods). Computer facilities and support were provided by the Commonwealth Center for Coastal Physical Oceanography at Old Dominion University. Eddie Haskell initially developed this copepod model, and his guidance on its application for this study is greatly appreciated. The insightful comments of the two reviewers stimulated significant improvements to this manuscript and are appreciated.

References

Ambler, J. W., and Miller, C. B. 1987. Vertical habitat-partitioning by copepodites and adults of subtropical oceanic copepods. Marine Biology, 94: 561–577.

Bartram, W. C. 1980. Experimental development of a model for the feeding of neritic copepods on phytoplankton. Journal of Plankton Research, 3: 25–51.

Bundy, M. H., Gross, T. F., Coughlin, D. J., and Strickler, J. R. 1993. Quantifying copepod searching efficiency using swimming pattern and perceptive ability. Bulletin of Marine Science, 53: 15–28.

Bundy, M. H., Gross, T. F., Vanderploeg, H. A., and Strickler, J. R. 1998. Perception of inert particles by calanoid copepods: behavioral observations and a numerical model. Journal of Plankton Research, 20: 2129–2152.

Demott, W. R., and Watson, M. D. 1991. Remote detection of algae by copepods: responses to algal size, odors and motility. Journal of Plankton Research, 13: 1203–1222.

Epp, R. W., and Lewis, W. M. 1980. The nature and ecological significance of metabolic changes during the life history of copepods. Ecology, 61: 259–264.

Evans, G. T. 1989. The encounter speed of moving predator and prey. Journal of Plankton Research, 11: 415–417.

Follows, M. J., Dutkiewicz, S., Grant, S., and Chisholm, S. W. 2007. Emergent biogeography of microbial communities in a model ocean. Science, 315: 1843–1846.

Fragopoulu, N., Siokou-Frangou, I., Christou, E. D., and Mazzocchi, M. G. 2001. Patterns of vertical distribution of *Pseudocalanidae* and *Paracalanidae* (Copepoda) in pelagic waters (0 to 300 m) of the eastern Mediterranean Sea. Crustaceana, 74: 49–68.

Franks, P. J. S. 2001. Turbulence avoidance: an alternate explanation of turbulence-enhanced ingestion rates in the field. Limnology and Oceanography, 46: 959–963.

Gargett, A. E. 1997. "Theories" and techniques for observing turbulence in the ocean euphotic zone. Scientia Marina, 61: 25–45.

Gaudy, R., Champalbert, G., and Le Borgne, R. 2003. Feeding and metabolism of mesozooplankton in the equatorial Pacific high-nutrient, low-chlorophyll zone along 180 degrees. Journal of Geophysical Research, 108; doi:10.1029/2000JC000743.

Goés, J. I., Thoppil, P. G., Gomes, H. D., and Fasullo, J. T. 2005. Warming of the Eurasian landmass is making the Arabian Sea more productive. Science, 308: 545–547.

González, H. E., Ortiz, V. C., and Sobarzo, M. 2000. The role of faecal material in the particulate organic carbon flux in the northern Humboldt Current, Chile (23 degrees S), before and during the 1997–1998 *El Niño*. Journal of Plankton Research, 22: 499–529.

Hansen, B., Bjornsen, P. K., and Hansen, P. J. 1994. The size ratio between planktonic predators and their prey. Limnology and Oceanography, 39: 395–403.

Haury, L. R., Yamazaki, H., and Itsweire, E. C. 1990. Effects of turbulence shear flow on zooplankton distribution. Deep Sea Research I, 37: 447–461.

Head, R. N., Medina, G., Huskin, I., Anadon, R., and Harris, R. P. 2002. Phytoplankton and mesozooplankton distribution and composition during transects of the Azores Subtropical Front. Deep Sea Research II, 49: 4023–4034.

Herman, A. W. 1989. Vertical relationships between chlorophyll, production and copepods in the eastern tropical Pacific. Journal of Plankton Research, 11: 243–261.

Hill, P. S., Nowell, A. R. M., and Jumars, P. A. 1992. Encounter rate by turbulence shear of particles similar in diameter to the Kolmogorov scale. Journal of Marine Research, 50: 643–668.

Hood, R. R., Laws, E. A., Armstrong, R., Bates, N. R., Brown, C. W., Carlson, C. A., Chai, F., *et al.* 2006. Pelagic functional group modeling: progress, challenges and prospects. Deep Sea Research II, 53: 459–512.

Huskin, I., Viesca, L., and Anadón, R. 2004. Particle flux in the subtropical Atlantic near the Azores: influence of mesozooplankton. Journal of Plankton Research, 26: 403–415.

Ikeda, T. 1985. Metabolic rates of epipelagic marine zooplankton as a function of body mass and temperature. Marine Biology, 85: 1–11.

Downloaded from https://academic.oup.com/icesjms/article-abstract/65/3/379/784056
by Old Dominion University user
on 15 May 2018

Incze, L. S., Hebert, D., Wolff, N., Oakey, N., and Dye, D. 2001. Changes in copepod distributions associated with increased turbulence from wind stress. Marine Ecology Progress Series, 213: 229–240.

Jenkinson, I. R. 1995. A review of two recent predation-rate models: the dome-shaped relationship between feeding rate and shear rate appears universal. ICES Journal of Marine Science, 52: 605–610.

Jiménez, J. 1997. Oceanic turbulence at millimeter scales. Scientia Marina, 61: 47–56.

Kiørboe, T., and Saiz, E. 1995. Planktivorous feeding in calm and turbulence environments, with emphasis on copepods. Marine Ecology Progress Series, 122: 135–145.

Kiørboe, T., and Thygesen, U. H. 2001. Fluid motion and solute distribution around sinking aggregates. II. Implications for remote detection by colonizing zooplankters. Marine Ecology Progress Series, 211: 15–25.

Landry, M. R., and Fagerness, V. L. 1988. Behavioral and morphological influences on predatory interactions among marine copepods. Bulletin of Marine Science, 43: 509–529.

Legendre, L., and Michaud, J. 1998. Flux of biogenic carbon in oceans: size-dependent regulation by pelagic food webs. Marine Ecology Progress Series, 164: 1–11.

Leising, A. W. 2001. Copepod foraging in patchy habitats and thin layers using a 2-D individual-based model. Marine Ecology Progress Series, 216: 167–179.

Lesieur, M. 1987. Turbulence in Fluids. Martinus Nijhoff Publishers, Dordrecht. 286 pp.

Maar, M., Nielsen, T. G., Stips, A., and Visser, A. W. 2003. Microscale distribution of zooplankton in relation to turbulence diffusion. Limnology and Oceanography, 48: 1312–1325.

Maar, M., Visser, A. W., Nielsen, T. G., Stips, A., and Saito, H. 2006. Turbulence and feeding behaviour affect the vertical distributions of *Oithona similis* and *Microsetella norvegica*. Marine Ecology Progress Series, 313: 157–172.

Mackenzie, B. R., Miller, T. J., Cyr, S., and Leggett, W. C. 1994. Evidence for a dome-shaped relationship between turbulence and larval fish ingestion rates. Limnology and Oceanography, 39: 1790–1799.

Marrasé, C., Costello, J. H., Granata, T., and Strickler, J. R. 1990. Grazing in a turbulence environment: energy dissipation, encounter rates, and efficacy of feeding currents in *Centropages hamatus*. Proceedings of the National Academy of Sciences, 87: 1653–1657.

Mazzocchi, M. G., and Paffenhöfer, G. A. 1999. Swimming and feeding behaviour of the planktonic copepod *Clausocalanus furcatus*. Journal of Plankton Research, 21: 1501–1518.

Metcalfe, A. M., Pedley, T. J., and Thingstad, T. F. 2004. Incorporating turbulence into a plankton foodweb model. Journal of Marine Systems, 49: 105–122.

Napp, J. M., Brooks, E. R., Matrai, P., and Mullin, M. M. 1988. Vertical distribution of marine particles and grazers. II. Relation of grazer distribution to food quality and quantity. Marine Ecology Progress Series, 50: 59–72.

Nival, P., and Nival, S. 1976. Particle retention efficiencies of an herbivorous copepod, *Acartia clausi* (adult and copepodite stages): effects on grazing. Limnology and Oceanography, 21: 24–38.

Paffenhöfer, G. A. 1972. The effects of suspended "red mud" on mortality, body weight, and growth of the marine planktonic copepod, *Calanus helgolandicus*. Water, Air, and Soil Pollution, 1: 314–321.

Paffenhöfer, G. A. 1984. Does *Paracalanus* feed with a leaky sieve? Limnology and Oceanography, 29: 155–160.

Paffenhöfer, G. A. 1998. On the relation of structure, perception and activity in marine planktonic copepods. Journal of Marine Systems, 15: 457–473.

Paffenhöfer, G. A., and Lewis, K. D. 1990. Perceptive performance and feeding behavior of calanoid copepods. Journal of Plankton Research, 12: 933–946.

Paffenhöfer, G. A., and Mazzocchi, M. G. 2002. On some aspects of the behaviour of *Oithona plumifera* (Copepoda: Cyclopoida). Journal of Plankton Research, 24: 129–135.

Paffenhöfer, G. A., Mazzocchi, M. G., and Tzeng, M. W. 2006. Living on the edge: feeding of subtropical open ocean copepods. Marine Ecology, 27: 99–108.

Paffenhöfer, G. A., Tzeng, M., Hristov, R., Smith, C. L., and Mazzocchi, M. G. 2003. Abundance and distribution of nanoplankton in the epipelagic subtropical/tropical open Atlantic Ocean. Journal of Plankton Research, 25: 1535–1549.

Peralba, A., and Mazzocchi, M. G. 2004. Vertical and seasonal distribution of eight *Clausocalanus* species (Copepoda: Calanoida) in oligotrophic waters. ICES Journal of Marine Science, 61: 645–653.

Peters, F., and Marrasé, C. 2000. Effects of turbulence on plankton: an overview of experimental evidence and some theoretical considerations. Marine Ecology Progress Series, 205: 291–306.

Price, H. J., Paffenhöfer, G. A., and Strickler, J. R. 1983. Modes of cell capture in calanoid copepods. Limnology and Oceanography, 28: 116–123.

Ramfos, A., Isari, S., Somarakis, S., Georgopoulos, D., Koutsikopoulos, C., and Fragopoulu, N. 2006. Mesozooplankton community structure in offshore and coastal waters of the Ionian Sea (eastern Mediterranean) during mixed and stratified conditions. Marine Biology, 150: 29–44.

Rothschild, B. J., and Osborn, T. R. 1988. Small-scale turbulence and plankton contact rates. Journal of Plankton Research, 10: 465–474.

Saiz, E., Calbet, A., and Broglio, E. 2003. Effects of small-scale turbulence on copepods: the case of *Oithona davisae*. Limnology and Oceanography, 48: 1304–1311.

Seuront, L. 2006. Effect of salinity on the swimming behaviour of the estuarine calanoid copepod *Eurytemora affinis*. Journal of Plankton Research, 28: 805–813.

Smith, S. L., and Madhupratap, M. 2005. Mesozooplankton of the Arabian Sea: patterns influenced by seasons, upwelling, and oxygen concentrations. Progress in Oceanography, 65: 214–239.

Steele, J. H., and Frost, B. W. 1977. The structure of plankton communities. Proceedings of the Royal Society of London, Series B, 280: 484–534.

Svensen, C., and Kiørboe, T. 2000. Remote prey detection in *Oithona similis*: hydromechanical versus chemical cues. Journal of Plankton Research, 22: 1155–1166.

Svensen, C., and Nejstgaard, J. C. 2003. Is sedimentation of copepod faecal pellets determined by cyclopoids? Evidence from enclosed ecosystems. Journal of Plankton Research, 25: 917–926.

Verity, P. G., Robertson, C. Y., Tronzo, C. R., Andrews, M. G., Nelson, J. R., and Sieracki, M. E. 1992. Relationships between cell volume and the carbon and nitrogen content of marine photosynthetic nanoplankton. Limnology and Oceanography, 37: 1434–1446.

Visser, A. W., Saito, H., Saiz, E., and Kiorboe, T. 2001. Observations of copepod feeding and vertical distribution under natural turbulence conditions in the North Sea. Marine Biology, 138: 1011–1019.

Visser, A. W., and Stips, A. 2002. Turbulence and zooplankton production: insights from PROVESS. Journal of Sea Research, 47: 317–329.

Webber, M. K., and Roff, J. C. 1995a. Annual biomass and production of the oceanic copepod community off Discovery Bay, Jamaica. Marine Biology, 123: 481–495.

Webber, M. K., and Roff, J. C. 1995b. Annual structure of the copepod community and its associated pelagic environment off Discovery Bay, Jamaica. Marine Biology, 123: 467–479.

Wiggert, J. D., Haskell, A. G. E., Paffenhöfer, G-A., Hofmann, E. E., and Klinck, J. M. 2005. The role of feeding behavior in sustaining copepod populations in the tropical ocean. Journal of Plankton Research, 27: 1013–1031.

Downloaded from https://academic.oup.com/icesjms/article-abstract/65/3/379/784056
by Old Dominion University user
on 15 May 2018

Woodson, C. B., Webster, D. R., Weissburg, M. J., and Yen, J. 2005. Response of copepods to physical gradients associated with structure in the ocean. Limnology and Oceanography, 50: 1552–1564.

Yamazaki, H., Mackas, D. L., and Denman, K. L. 2002. Coupling small-scale physical processes with biology, pp. 51–112. *In* The Sea. Ed. by A. R. Robinson, J. J. McCarthy, and B. J. Rothschild. Wiley and Sons, New York.

Yen, J. 2000. Life in transition: balancing inertial and viscous forces by planktonic copepods. Biological Bulletin, 198: 213–224.

doi:10.1093/icesjms/fsm193

Downloaded from https://academic.oup.com/icesjms/article-abstract/65/3/379/784056
by Old Dominion University user
on 15 May 2018